

## Research

### Fibroblastic tissue growth on polymeric electrospun membranes: a feasibility study

Luana A. Osório<sup>1</sup> · Angel Naveenathayalan<sup>1</sup> · Elisabete Silva<sup>2</sup> · Ruth E. Mackay<sup>1</sup>

Received: 22 February 2024 / Accepted: 18 June 2024

Published online: 25 June 2024

© The Author(s) 2024 [OPEN](#)

#### Abstract

In recent years the interest in synthetic scaffolds has increased significantly as an alternative to animal-derived materials, as well as the advancement of material and manufacturing engineering, has resulted in improved standardisation and reproducibility within the field. Despite these advancements, a significant amount of research on animal-derived scaffolds, whilst research on synthetic materials is lacking for the growth of non-tumourgenic breast cell lines. The main objective of this work is to manufacture biodegradable scaffolds using biocompatible materials such as PVA (Polyvinyl Alcohol), PU (Polyurethane), Ge (Gelatin) and PCL (Poly( $\epsilon$ -caprolactone) to test human cell adhesion and investigate the optimal system that supports representative tissue organisation and that could be used as an alternative to Matrigel™. Here, human mammary fibroblasts (HMF) were used as proof of concept. The membranes were manufactured using the process of electrospinning and characterised by scanning electron microscopy (SEM), Fourier transforms infrared spectroscopy (ATR-FTIR), contact angle, tensile strength, and degradation studies. The assessment of the membranes as a viable biomaterial for the growth and development of cells was studied by MTT proliferation assay, fluorescence microscopy and SEM imaging. Results demonstrate that all materials are suitable for HMF proliferation. However, from microscopy analysis, only PU and PVA membranes induced morphological organisation of HMF similar to those results obtained in the Matrigel™ control conditions. This feasibility study reveals that HMF organisation, and proliferation are affected by the properties of the scaffold. Consequently, scaffolds parameters should be adjusted and manipulated to impact cell behaviour and emulate in vivo conditions.

#### Article Highlights

- This work shows human mammary fibroblasts (HMF) grown on a selection of electrospun membranes to find the optimal substrate.
- The biodegradable polymeric membranes (PU, PCL/PU, PCL/Ge and PVA) were chosen to avoid the use of expensive alternatives such as Matrigel.
- It was found that the human mammary fibroblasts proliferated and organised themselves depending on scaffold properties, such as porosity, fibre diameter and wettability.

---

✉ Ruth E. Mackay, [ruth.mackay@brunel.ac.uk](mailto:ruth.mackay@brunel.ac.uk) | <sup>1</sup>Department Mechanical and Aerospace Engineering, Brunel University London, Kingston Lane, London UB8 3PH, UK. <sup>2</sup>Francis Crick Institute, Midland Road, London NW1 1AT, UK.



## 1 Introduction

When using *in vitro* models, the understanding of disease's aetiology is vastly dependent on the models' ability to replicate the disease's microenvironment. The stromal microenvironment is well known for being critical in the regulation of mammary gland development and tumorigenesis [1]. The mammary gland is a heterogeneous tissue formed by a variety of cell types, each with different functions and roles in the development and tissue maturation that form complex network interactions. The stroma that surrounds the functional epithelium, not only provides physical support but also transmits signalling cues to the epithelium through the transmembrane receptors, which facilitates the maintenance of tissue integrity. The stroma includes cellular components, such as fibroblasts, immune cells, endothelial cells, adipose, inflammatory cells, and extracellular matrix (ECM) [2]. Mammary stromal fibroblasts are responsible for the maintenance of extra cellular matrix (ECM) homeostasis and the modulation of cell polarity and growth control [3]. Even though the epithelium has the most tumorigenic and invasive potential, it has been proven that the stroma plays role in cancer development. The role of the stroma on mammary tumorigenesis was first described 40 years ago by DeCosse et al., (1975), when mesenchyme tissues were shown to induce cytodifferentiation in murine tumour cells, resulting in the interactions between the cell types that lead to gene expression changes and tumour mass formation [4].

Fibroblasts are cells that form the loose connective tissue surrounding the epithelial sheet, responsible for mesenchymal lineage maintenance, tissue synthesis and immune regulation [5, 6]. These cells are responsible for the active support of epithelial structures and secretion of important molecules like fibroblast growth factor (FGF) and ECM proteins (collagen, fibronectin, laminin, and collagen I, II and IV) and secretion [5]. Fibroblasts have been reported to play an enabling role in the carcinogenic process since they are responsible for the production and deposition of the tumour stroma ECM [7]. Several studies have observed the recruitment of breast cancer-associated fibroblasts (BCAFs) to induce changes to the tumour microenvironment (TME), thus enhancing cancer dissemination [8]. As an example, El-Ashry's group has demonstrated the combination of BCAFs and cancer cell aggregates has the ability to circulate towards peripheral blood in breast cancer metastatic patients [9].

Over the past few decades, the interaction between normal and aberrant fibroblasts has been directly recognised to play critical protective roles or as breast cancer initiators. Kupperwasser's study revealed that fibroblasts that overexpress TGF- $\beta$  and HGF are linked to higher incidences of breast tumours [10]. On the other hand, normal fibroblasts also have been shown to have a protective role, with the ability to suppress oestrogen-induced growth of preneoplastic breast EIII8 cells [11]. Based on the significant role fibroblasts play in breast carcinogenesis, it is imperative that these cells are included in *in vitro* breast cancer models in a way that recapitulates their behaviour and cellular interactions in human tissues.

Conventionally, *in vitro* breast tissue models vastly rely on 2D monolayer cultures. However, these do not reliably represent the complex cellular interactions of heterogenous tissues in 3D microenvironments. In recent years, attempts have been made to use synthetic scaffolds as a framework to seed mammary stromal cells such as chitosan-alginate and Matrigel™/collagen mixtures [12, 13]. Nevertheless, the wide range of synthetically produced scaffolds available introduces complexities that impede the analysis and comparative assessment of research data across various studies [13].

Interest in synthetic polymers has vastly risen in the past decade due to the potential of customising their characteristics to the needs of different cell and tissue types. A plethora of polymeric materials have been used to manufacture synthetic scaffolds within tissue engineering, as well as other manufacturing fields [14]. Given the versatility of their composition and manufacturing methods, these materials can provide the conditions for the culture of diverse types of cells and replicate physiological and anatomical conditions [15]. Most of the materials used to replicate the natural ECM in three-dimensional models take advantage of naturally derived materials, such as Matrigel™, since these emulate *in vivo* composition (laminin, fibronectin, Collagen IV and entactin) and stiffness, and can enhance cell viability and proliferation [16, 17]. Nevertheless, these have batch-to-batch variability, low stability and poor mechanical properties that result in rapid degradation rates influencing cell fate [18]. While the scaffold material is critical for cell viability and ECM characteristics, the technique used in the scaffold production also impacts cell growth and tissue structure, as it defines the scaffold's mechanical properties, fibre diameter and porosity [19]. As such, technologies within additive manufacturing, such as 3D bioprinting, fused deposition modelling (FDM) and electrospinning, have optimised the way scaffolds are designed and constructed to fit specific requirements of cellular tissue and their dynamic microenvironment [20], whilst providing a standardised scaffold that maintains its biochemical properties across batches and hence providing consistent and reproducible cell culture experiments to advance scientific research with greater accuracy and confidence [17].

Electrospinning is one of the most widely used techniques to produce scaffolds, as it is not only a simple and cost-efficient method but also allows for the production of a wide array of polymeric materials with a fibre diameter ranging from 2 nm to tens of micrometres [19, 21]. This technique is an uncomplicated and low-cost alternative to additive manufacturing that benefits from the mechanical properties of a variety of polymers [22]. It presents an electrodynamic procedure that takes advantage of an electrostatic field between the needle tip and a ground collection plate, inducing a charge on the dielectric polymeric solution chosen. The formation of a structure known as a Taylor cone, where nanofibres start forming, depends on the charge applied to the droplets and dielectric characteristics of the polymeric solution [21, 23]. The versatility of this technique is directly linked to the manipulation of parameters that can affect the quality of the spinning, such as the solution parameters (viscosity and electrical resistivity), procedure parameters (distance to collector, flow rate and voltage) and surrounding environment conditions (humidity and temperature) [24].

Electrospun membranes possess a distinctive fibro-porous structure that forms a nanoscale/microscale architecture of interconnected pores like the natural ECM enabling the creation of a viable synthetic functional tissue-like scaffold. A good example of this is the interconnectivity of pores that enable cell migration and nutrient trade detected in the skin and bone tissue [25, 26]. Moreover, the good mechanical stability of these membranes has rendered them a viable host for the formation of blood vessels, cartilage and skeletal muscle, neural and other types of soft tissues [21]. Nonetheless, due to the variability of spinning parameters and materials available, there is still a lack of standardisation of manufacturing parameters for specific tissues [27].

Polymers are commonly used as biomaterials across a variety of biomedical fields for their simplicity of production, flexibility, and biocompatibility [27]. Synthetically-derived materials are inexpensive substitutes for naturally derived biomaterials [28]. Among the most used ones are Poly( $\epsilon$ -caprolactone) (PCL). PCL is a linear aliphatic and biodegradable polyester that has been regulated by the BS ISO 10993 and 13,781 as safe for biomedical and tissue engineering applications [29, 30]. Despite being vastly used for co-cultures [31], this biomaterial is hydrophobic which reduces cell adherence and interaction [32]. Hence, there is a need to combine this polymer with other materials, such as gelatin and polyurethane, to increase biocompatibility. Gelatin (Ge) is acquired by the hydrolysis and denaturation of animal skin, making it an exceptionally biocompatible and biodegradable material [33]. Gelatin composite scaffolds have been reported to successfully sustain synthetic vascularisation formation [34, 35]. It is known to be highly biocompatible due to its cell-binding motifs such as, RGD and porous structure that closely resembles natural ECM [36]. Additional biomaterials that are used in tissue engineering include Polyurethane (PU) and Polyvinyl Alcohol (PVA) for their low-cost fabrication, biocompatibility, and advantageous mechanical properties [37, 38]. Similar to PCL, PU is a linear polymer with an analogous functional group and is known to increase cellular attachment [39]. PVA is a vinyl polymer used as the backbone of tissues such as bone, vascular and neural due to its mechanical performance, biocompatibility, and wettability [38].

The development of these scaffolds was inspired by the need for an alternative to Matrigel™ for the study of co-culture of breast tissues (epithelial, stromal and endothelial). For this study, Human Mammary Fibroblast (HMF) were used as proof of concept for the initial development of the scaffolds. To limit the permutations of materials used for this study, PCL, PU, PVA and Ge were selected due to their documented advantages across a spectrum of tissue types, increasing the odds of successful outcomes. The scaffolds were manufactured using electrospinning techniques. The mechanical properties of the membranes were characterised using SEM, tensile strength tests and degradability/wettability assays. In order to understand the effect, the manufacture scaffolds have on cellular behaviour, cell viability studies were undertaken. Our results, demonstrate that the proposed scaffolds have the potential to be used as a replacement for Matrigel™ and emulate in vitro behaviour. In the next section, we outline the methods employed for the manufacture and study of the various electrospun scaffold candidates. In Sect. 3 we present the comprehensive results regarding mechanical characterisation of the membranes, clarifying the influence of their architecture on cell behaviour and organisation, followed by an in-depth discussion of these findings.

## 2 Methodology

### 2.1 Solutions for electrospinning

A solution containing 4% (w/v) Polyurethane (PU) (Sigma Aldrich, UK) was prepared by dissolving pellets in 1:1 ratio with methanol (32.04 g/mol, ThermoFisher, UK) and chloroform (119.38 g/mol, ThermoFisher, UK), this was stirred using a magnetic stirrer for a minimum of 16 h. For the PVA (Mw 89,000–98,000, Sigma Aldrich, UK), a 10% (w/v) solution was dissolved using deionised water (DI) and stirred at 70 °C overnight, followed by the addition of 20% of the final volume

of 70% ethanol and stirred for a further 4 h; this was then stirred using a magnetic stirrer for a minimum of 16 h. For the blended solutions, 4% (w/v) PU and 4% (w/v) PCL (Mn 80,000, Sigma Aldrich, UK) were dissolved by stirring in tetrafluoroethylene (TFE) (100.04 g/mol, ThermoFisher, UK) overnight. For the composite solution, 4% (w/v) Ge from porcine skin type A (Sigma Aldrich, UK) and 8% (w/v) PCL solutions were dissolved separately in TFE and combined 24 h later using 100  $\mu$ L of acetic acid (AA) ( $\geq 99.7\%$ , Sigma Aldrich, UK) per 10 mL of prepared solution; this was then stirred using a magnetic stirrer for a minimum of 16 h. Gelatin was selected as a positive control material for the electrospinning process due to its well-established reputation as a highly biocompatible material and propensity for cell adhesion and proliferation. All the solutions were placed in an ultrasonic bath for 30 min before the electrospinning process to eliminate any bubbles and remaining pellets.

## 2.2 Scaffold fabrication

The electrospinning machine consisted of custom-made setup by AC solutions Ltd, UK and a syringe pump Fusion 100 (KR Analytic, UK) represented in Fig. 1. The parameters for electrospinning were tested until reliable formation of nanofibres was achieved and the solutions were prepared as follows. All the scaffolds were produced using a 22G needle, at room temperature (23 °C) and a 19 cm distance from the collection plate. The individual settings were as follows:

- PU scaffolds: voltage of 17.5 kV, flow rate of 1.5 mL/h with relative humidity of  $\sim 70\%$ .
- PU/PCL composite scaffolds: voltage of 12.5–15 mL/h,  $\sim$  humidity 40%.
- PCL/GE composite scaffolds: voltage of 12.5–15 mL/h,  $\sim$  humidity 75%.

The PVA scaffolds were manufactured using the same needle gauge and temperature but at a 16 cm distance from the collection plate with a voltage of 17.5–22.5 kV, flow rate of 0.8 mL/h and humidity of  $\sim 40\%$ .

## 2.3 Crosslinking

The crosslinking process was carried out for the composite scaffolds made of PVA and Gelatin, due to the mechanically weak and unstable nature of these polymers when exposed to water-based solutions. 10% (w/v) PVA scaffolds were placed in a vacuum oven at 150 °C for 2 h to crosslink the fibres using heating. 8%/4% (w/v) PCL/Ge composite scaffolds

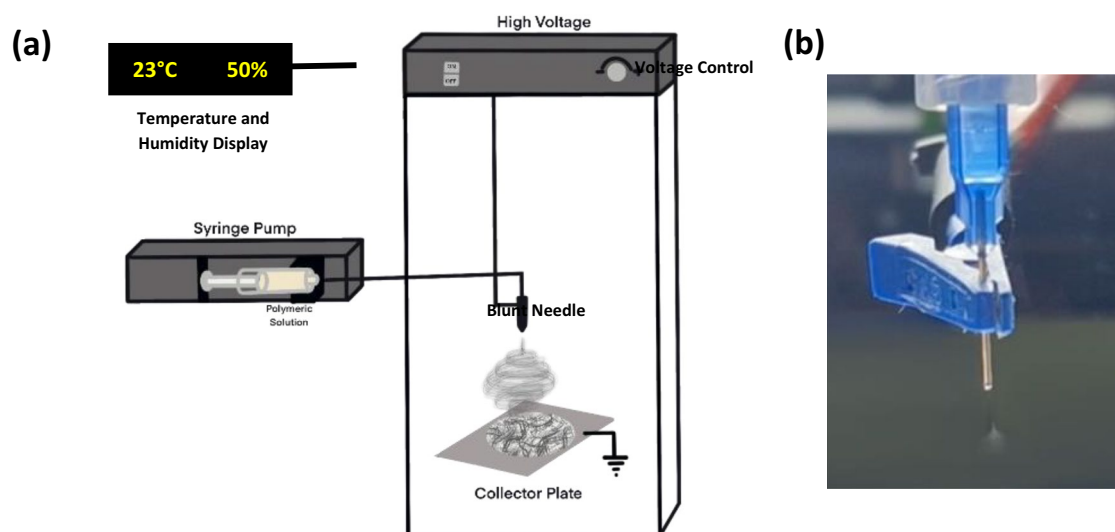


**Fig. 1** Visual representation of the electrospinning process. **a** Schematic representation of the electrospinning process and the equipment used to create electrospun membranes. Polymeric solution is pushed through the system using a syringe pump, the electric field applied within the chamber creates a spinneret where the solvent evaporates and leads to the formation of polymeric fibres, that are directed towards a grounded plane collector; **b** Formation of the Taylor cone at the spinneret of a 22G when exposed to an adequate voltage and nanofibre formation, this demonstrates the formation of fibres from 3%/3% (w/v) PCL/PU

were chemically crosslinked with glutaraldehyde (GA) vapour using 10 ml of 25% aqueous GA solution in a vacuum desiccator for 3 days.

## 2.4 Scaffold morphology

To obtain the morphology analysis of the scaffold surface, a sample of 10 × 10 mm was prepared and sputter coated with gold for 30 s using a Polaron SC7640 Sputter coater to generate a conductive sample. Samples were screened under a Scanning Electron Microscope (SEM) (Jeol IT200) at 1400 × magnification and an acceleration voltage of 10 kV.

## 2.5 Fibre diameter and pore size

The average fibre diameter ( $\mu\text{m}$ ) and average pore size ( $\mu\text{m}^2$ ) were determined using the images acquired on the SEM Jeol IT200. The measurements of each parameter were performed using ImageJ (Version: 1.53 k, University of Wisconsin, Madison, WI, USA); an example is shown in Fig. 2. For the fibre diameter, a total of 500 random measurements were undertaken on 5 different SEM images of each type of scaffold. To calculate the pore size of each scaffold manufactured, a total of 100 measurements were taken of random pores' area on 5 SEM images. The final data was analysed using GraphPad Prism (version 8.4.3, Dotmatics, Boston) to determinate the mean values.

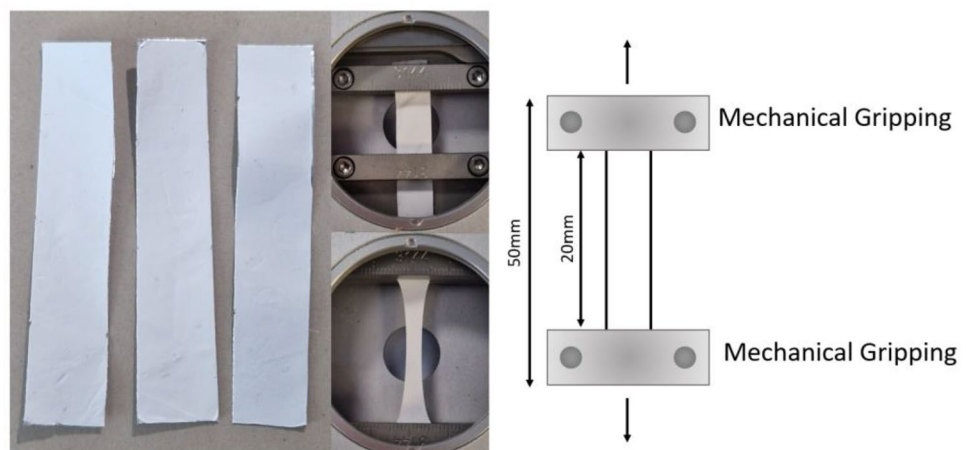
## 2.6 Contact angle measurements

Contact angle provides information regarding how hydrophilic the surface of the sample is. The wettability of the nanofibrous scaffolds was calculated by measuring the static contact angle formed by a drop of distilled water on a 1 × 1 cm flat scaffold. The First Ten Angstroms instrument had a perpendicular syringe with a needle of 30G (Inner Diameter (ID) 0.121 mm and outer diameter (OD) 0.305 mm) and a camera that captured the scaffold/water interaction. Five seconds later, an image was captured and analysed using FTA32 video-based goniometer software (Version: 2.0, First Ten Angstroms). This procedure was undertaken 4 times, and results are displayed by the mean with standard error bars.

## 2.7 Tensile strength

The mechanical tensile strength of each scaffold was measured using a uniaxial Tensile Stress Testing Stage (T96S, Linkam Scientific Instruments, UK) equipped with a 20N load cell which was applied at a velocity of 250  $\mu\text{m/s}$ . All samples were prepared in a rectangular shape with the dimensions of 10 × 50 mm scaffold strips and clamped across a 20 mm distance between the compression grips in the y-axis (Fig. 2). The thickness of each sample was measured by clamping the selected strip between two glass slides and placed in the SEM Jeol IT200 at 1400 × magnification and an acceleration voltage of 10 kV, the thickness of each sample was then measured using ImageJ (Version: 1.53 k, University of Wisconsin, Madison, WI, USA). The measurements of each sample were entered into the LINK Control software (Linkam Scientific Instruments,

**Fig. 2** Scheme of sample preparation and tensile testing



UK) was used to accomplish the mechanical testing. Young's Modulus was derived from the slope equation (Eq. 1) applied to the linear elastic region evident in the stress–strain profiles of each individual samples.

$$\text{Young's Modulus} = \frac{\sigma_2 - \sigma_1}{\varepsilon_2 - \varepsilon_1} \quad (1)$$

Stress ( $\sigma$ ) represents the force applied divided by the cross-sectional area and strain ( $\varepsilon$ ) represents the elongation of the material divided by its original length.

## 2.8 Infrared spectroscopy

To examine the functional groups and fibre composition in the different polymeric scaffolds, a Fourier Transform Infrared Spectroscopy (FTIR) was employed. This analysis encompasses both pre and post-crosslinking data, as relevant to the context, the FTIR analysis was undertaken using the PerkinElmer Spectrum One FT-IR Spectrometer and Spectrum IR software (Version: 10.7.2.1630), manufactured by Perkin Elmer, USA. All Spectra were recorded in the wavelength range of 4000–600  $\text{cm}^{-1}$  over 32 scans.

## 2.9 Degradation procedure

To examine the stabilisation of the manufacture scaffolds, the weight loss was assessed. The scaffolds were cut in a square shape of 10 × 10 mm and were immersed in Phosphate-Buffered Saline (PBS) in incubation conditions (37 °C and 5% CO<sub>2</sub>) to emulate the growth of biological tissue over a period of 30 days. The samples were removed from the solution at different time points (0, 15 and 30 days) and rinsed twice with distilled water to remove any dust that may have accumulated. These were left to dry at room temperature to evaporate the remaining liquid. The scaffolds were then weighted, and the weight degradation was calculated using the following equation (Eq. 2), where  $W_0$  represents the initial weight and  $W_t$  is the weight at the different data points. This process was repeated three times. Displayed results represent the mean and standard error bars.

$$\text{Weight loss(\%)} = \frac{W_0 - W_t}{W_0} \times 100 \quad (2)$$

pH was measured at each data point using Corning M240 pH meter (Corning, UK), to assess the effect of degradation by-products on the acidity of the PBS against a PBS control sample. The analysis was repeated three times to calculate the mean and standard error of each scaffold degradation.

### 2.9.1 Cell line and routine cell culture

Primary human mammary fibroblasts (HMFs) were obtained from ScienCell (Buckingham, UK) and maintained as recommended by the supplier's instruction in a 75  $\text{cm}^2$  canter-neck tissue culture flask (Greiner, Gloucestershire, UK). Cells were grown with Dulbecco's Modified Eagle Medium (DMEM/F12; Invitrogen, Paisley, UK), supplemented with 5% horse serum (Invitrogen, UK), 5% Foetal Bovine Serum (FBS), 20 ng/mL of epithelial growth factors (EGF), 100 ng/mL cholera toxin, 0.5  $\mu\text{g}/\text{mL}$  hydrocortisone, 10  $\mu\text{g}/\text{mL}$  insulin and 1% Penicillin/Streptomycin (P/S). All reagents were purchased from Sigma-Aldrich (Dorset, UK) unless listed otherwise.

HMF cells were seeded at a density of  $5 \times 10^5$  cells/flask and kept in a humidified incubator at 37 °C and 5% CO<sub>2</sub>. Medium was replaced every three days until 70% confluence was achieved followed by the passaging with 0.25% trypsin–EDTA up to a maximum of 10 passages.

### 2.9.2 Scaffold cell culture

The scaffold was cut into 10 × 10 mm squares (three replicates for each condition) and placed in non-adherent cell culture 24-well plates (Sarstedt, Nümbrecht, Germany). The process of sterilisation was achieved by submersion of the scaffolds in 70% ethanol solution and three washes with phosphate-buffered saline (PBS) (ThermoFisher, UK), followed by exposure to ultraviolet (UV) light for 30 min in the now sealed plates.

Solutions with adequate cell density were prepared (10,000 cells/well) in the previously described medium and 500  $\mu\text{L}$  were pipetted drop by drop over the centre of the scaffold to ensure a homogeneous coverage of the scaffold. Finally, the seeded scaffolds were incubated overnight to ensure cell attachment at 37 °C and 5%  $\text{CO}_2$  atmosphere, and the medium was changed the following day.

Three-dimensional Matrigel™ cell cultures were performed as a control condition since it is a highly biocompatible animal-derived material and is widely used across breast cancer research [40]. To reduce the effect of batch-to-batch variation, a mixture of different concentrations of growth factor reduced (GRF) Corning® Matrigel™ matrix was prepared with a final concentration of 11.6 mg/mL. A volume of 150  $\mu\text{L}$  of Matrigel™ was then pipetted into the 24-well plates using cooled pipette tips, previously placed in a –20 °C freezer, to avoid gel clumping and allowed to polymerise for 15 min in the incubator. Cells were then seeded using the same methodology and the same concentration (10,000 cells/well) as the scaffold conditions.

### 2.9.3 Cell proliferation assay

The MTT assay was performed to assess cell proliferation on the manufactured scaffolds and Matrigel™ cell culture plates. MTT is a colourimetric assay that depends on the transformation of yellow tetrazolium salt into water-soluble purple crystals of formazan by the viable cells in the culture. The 10 × 10 mm scaffolds were placed in 24-well plates and sterilised, followed by Matrigel™ pipetting and cell seeding using protocols described in the previous section. The plated cell cultures were maintained for 7 days with medium changes every two days. After 72 (3 days), 120 (5 days) and 168 h (7 days), the samples were collected and an MTT assay was undertaken. The cell culture medium was removed and 500  $\mu\text{L}$  of MTT solution was added and incubated for 4 h in culture conditions. The samples were then briefly washed with PBS to reduce non-specific crystal formation. The crystals formed in the samples were dissolved using dimethyl sulfoxide (DMSO) and the plates were then left on a shaker for 20 min protected from any light exposure. 200  $\mu\text{L}$  aliquots from each replicated well were transferred into a 96-well plate and 200  $\mu\text{L}$  DMSO were pipetted as a blank. The absorbance of each well was read at 570 nm using a microplate reader (ELx808™ Incubating Absorbance Plate Reader, BioTek Instruments, USA). The results were calculated following (Eq. 3). to assess the percentage of cellular growth and plotted using GraphPad Prism (version 8.4.3, Dotmatics, Boston). A two-way ANOVA Dunnett's multiple comparison test was applied to the ImageJ collected data for analysis of statistical significance. Error bars represent the standard error of the mean for each condition.

$$\text{Cellular Growth (\%)} = \frac{\text{Absorbance Reading}}{\text{Matrigel Absorbance at 168h}} \times 100 \quad (3)$$

### 2.9.4 Fluorescence microscopy

To observe cellular growth and morphological behaviour on the nanofibrous scaffolds, the samples were stained with DAPI and Phalloidin. Scaffolds were cut in 10 × 10 mm and placed in non-adherent cell culture 6-well plates (Sarstedt, Nümbrecht, Germany) for easier removal and cultured for 7 days. The scaffolds and Matrigel™ samples were fixated using 4% paraformaldehyde (ThermoFisher, UK) for 15 min at room temperature, followed by three washes in PBS. The samples were permeabilised with Acetone (Sigma-Aldrichdorset, UK) for 15 min at –20 °C and washed with PBS three times. Samples were blocked in 1% bovine serum albumin (BSA) solution (Sigma-Aldrich, UK) for 45 min and once again washed three times with PBS. The cells were stained using Alexa Fluor™ 594 Phalloidin (ThermoFisher, UK) for 60 min at room temperature and washed three times with PBS. Finally, all the samples were stained and mounted using VECTASHIELD® Hardset Antifade Mounting Medium with DAPI (Vector Laboratories, Cambridge, UK). Samples were observed under a Leica DM4000 fluorescent microscope.

### 2.9.5 Cellular scanning *electron* microscopy (SEM)

SEM imaging was used to observe interactions between the cell colonies and the surface architecture of the scaffolds. Cell cultures were grown in scaffolds for 7 days according to the methodology previously described. The specimens were collected and washed with PBS three times to remove any remaining medium followed by dehydration with graded concentrations of ethanol (50%, 70%, 90% and 100%, v/v) for 5 min each step. After drying, the samples were sputter

coated with gold for 30 s using a Polaron SC7640 Sputter coater to generate a conductive sample. Samples were screened under a SEM Jeol IT200 at 1600× magnification and an acceleration voltage of 10 kV.

### 2.9.6 Morphological analysis

HMF structures in Matrigel™ were imaged using a Leica DMI1 Inverted Microscope (Leica Microsystems, UK). HMF structures in the scaffolds were imaged using the previously mentioned protocols. Measurements of 5 randomly selected spheroids were then taken in two separate experiments and analysis was carried out using ImageJ and statistical analysis was undertaken on GraphPad (version 8.4.3, Dotmatics, Boston). A one-way ANOVA with Dunnett's multiple comparison test was applied to the ImageJ collected data for analysis of statistical significance. Error bars represent the standard error of the mean for each condition.

## 3 Results

### 3.1 Electrospinning parameters

Each of the relevant parameters for the quality of the electrospun scaffold (solvent type, flow rate, voltage, distance between spinneret and the collector plate and the concentration of the desired solutions) were studied and optimised for the laboratory environment conditions and equipment using the following polymers—PU, PCL, Ge and PVA [21, 24, 33, 41–46]. These parameters were individually changed to understand the influence on the quality of spinning.

#### 3.1.1 Optimisation of the electrospinning process

To understand the impact of different parameters on the fibre and pore structures of electrospun scaffolds, different polymer mixtures were prepared with a variety of solvents such as tetrafluoroethylene (TFE), 70% ethanol, methanol, and chloroform on each material described above. A plethora of other solvents described in the literature, such as N, N-dimethylformamide (DMF) and tetrahydrofuran (THF), were also used when testing solutions [47]. Nonetheless, the electrospinning process generated variable parameters from each manufacturing attempt. Firstly, an elimination process was carried out to exclude solutions that did not lead to the creation of a Taylor cone followed by the deposition of uniform nanofibres on the collector plate under any voltage, height, and flow rate. The quality of the polymer concentration and solution viscosity can be assessed by the lack, formation or droplets produced on the nanofibres. For example, lower concentrations of polymeric solution led to the breakage of the polymer chain and subsequent bead formation. To find the critical value of applied voltage and flow rate for each polymeric solution, a range of 10 to 25 kV and 0.5 to 2 (mL/h) were tested until elongated nanofibres that did not contain droplets started forming [44].

Flow rates between 0.1 to 0.8 mL/h generated no fibres, and 0.8 to 1.5 mL/h flows showed fibre formation with a stabilised Taylor cone showing reduced beading for 10% PVA. Higher flow rates i.e. > 1.5 mL/h generated sizable droplets that were too large to suspend at the tip of the spinneret and as a result fell freely onto the collector plate, leading to the formation of large beads, disrupting the membrane. The applied voltage and the distance between the spinneret tip and the collector plate are dependent, with lower distances requiring less applied voltage for Taylor cone formation due to the dielectric value of the solution. Parameters like humidity were shown to play a vital role in the viscosity of certain membranes such as the PU and Ge requiring higher humidities to reduce the viscosity at the spinneret tip and start the formation of the Taylor cone. Nonetheless, this parameter was hard to control in the set up used.

This process was then followed by the examination of the electrospun scaffold under SEM imaging to examine the quality of fibre and pore sizes for cellular growth and attachment, resulting in the shortlisting of 4 candidates manufacturing using the conditions described in Table 1.

Based on the extensive electrospinning process and experiment optimisation, a variety of membranes can be generated when different parameters are adjusted. The composition of the solution and electrospinning parameters will dictate the size and morphology of the fibres manufactured. The morphology, fibre diameter and pore size distribution histograms for each of the optimised electrospun membranes are presented in Fig. 3.

Surface morphology assays revealed that the addition of PCL to the PU scaffold resulted in smaller mean fibre diameter from  $569 \pm 277$  nm to  $262 \pm 148$  nm and smaller pore size from  $3109 \pm 2413$  nm<sup>2</sup> to  $1807 \pm 1116$  nm<sup>2</sup>, as demonstrated in Fig. 3a and c. As shown in Fig. 3b, 8%/4% (w/v) PCL/GE scaffolds were revealed to have the highest fibre diameter at

**Table 1** Electrospinning parameters for the shortlisted membranes

Polymer Concentrations (w/v)	Solvent	Flow Rate (mL/h)	Voltage (kV)	Temperature (C°)	Humidity (%)	Distance (cm)	Needle (G)	Crosslinking
8% PCL/4% Ge	TFE	0.8	12.5–15	22–24	70–80	19	22	GA for 72 h
3% PCL/3% PU	TFE	0.8	12.5–15	22–24	40–50	19	22	N/A
4% PU	Methanol/ chloroform	1.5	17.5	22–24	70–80	19	22	N/A
10% PVA	Water	0.8	17.5–22.5	22–24	40–50	16	22	Heat 150 °C for 2 h

384 ± 127 nm and pore sizes of around 4800 ± 2289 nm<sup>2</sup>. On the other hand, 10% (w/v) PVA scaffolds were associated with higher beading density and small fibre diameter (176 ± 59 nm), organised in aleatory folding structure with pore sizes of around 233 ± 354 nm<sup>2</sup> as it can be seen in Fig. 3d.

### 3.2 Chemical structure and residual solvent evaluation using FTIR spectroscopy

FTIR analysis is commonly utilised to explore functional groups and potential interactions within compound structures. In this study, the functional groups of PCL/Ge, PCL/PU, PU and PVA (pre- and post- crosslinking, as relevant to the context) were examined to characterise the composition of the fabricated scaffolds, shown in Fig. 4.

Figure 4c represents the FTIR results for the 4% PU-manufactured scaffolds. This membrane shows a medium peak at the 3314 cm<sup>-1</sup> for the –NH group (stretching of urethane linkage (–NHCOO–), 1715 cm<sup>-1</sup> for amide I, 1530 cm<sup>-1</sup> for amide II and 1230 cm<sup>-1</sup> for amide III bonds, all very characteristic of polyurethane bonds. Moreover, peaks at 2941 cm<sup>-1</sup> and 2853 cm<sup>-1</sup> were registered from the asymmetric and symmetric vibration of the group –CH<sub>2</sub> [48],

These results are also visible on the 3% PCL/ 3% PU scaffold (Fig. 4a) distinctive PCL peaks recorded at 1722 cm<sup>-1</sup> and 1187 cm<sup>-1</sup> for the C–O and C–O–C stretching bands in PCL ester bonds, respectively [49]. The peaks at 2940 and 2859 cm<sup>-1</sup> demonstrate the presence of common functional groups between both polymers. This data is corroborated by Cruz-Maya et al., where PCL derived scaffolds present distinctive peaks at 1727 cm<sup>-1</sup> and 1170 cm<sup>-1</sup> which correspond to C–O and C–O–C stretching bands. These membranes also display common functional group around 2949 cm<sup>-1</sup> and 2865 cm<sup>-1</sup> [50]. Showcasing that the addition of PU does not significantly alter the chemical structure of the PCL and maintains its mechanical properties.

In Fig. 4b the PCL/Ge results spectrum exhibited the expected protein bands at 3299 cm<sup>-1</sup> (–NH group), 1723 cm<sup>-1</sup> (amide I), 1548 cm<sup>-1</sup> (amide II) and 1238 cm<sup>-1</sup> (amide II) similar to the results obtained by Kuppan et al., alongside the bands associated to PCL 2944 cm<sup>-1</sup> (CH<sub>2</sub> stretching), 2867 (CH<sub>2</sub> stretching), –1723 cm<sup>-1</sup> (carbonyl stretching) and 1293 cm<sup>-1</sup> (C–O and C–O stretching) consistent with results in the literature, showing the adjustment of the Gelatin to the PCL characteristics [51, 52]. The uncrosslinked samples show similar wavelength peaks but with increased transmittance suggesting fewer bonds and therefore, lower stability.

Results for the 10% PVA scaffold spectrum are displayed in Fig. 4d, this reveals absorption and a strong broad peak at 3271 cm<sup>-1</sup> (O–H stretching), along with a peak at 2914 cm<sup>-1</sup> (–CH<sub>2</sub> stretching). Other relevant peaks include 1373 cm<sup>-1</sup> for C–H and O–H bending peaks similar to results reported on PVA electrospun membranes [53]. Similar to the uncrosslinked version of the PCL/Ge electrospun membranes, the PVA uncrosslinked membrane also presents stronger peaks when compared with the crosslinked.

### 3.3 Surface contact angle measurements

The contact angle for the different composition electrospun scaffolds was found to range from 20 to 89° (Fig. 5b). The measurements were acquired in triplicates and statistical analysis was performed. 3%/3% PCL/PU and 4% PU demonstrated higher contact angles of 71.07 ± 2.41° and 88.37 ± 0.96° respectively. 8%/4% PCL/Ge created a droplet with an

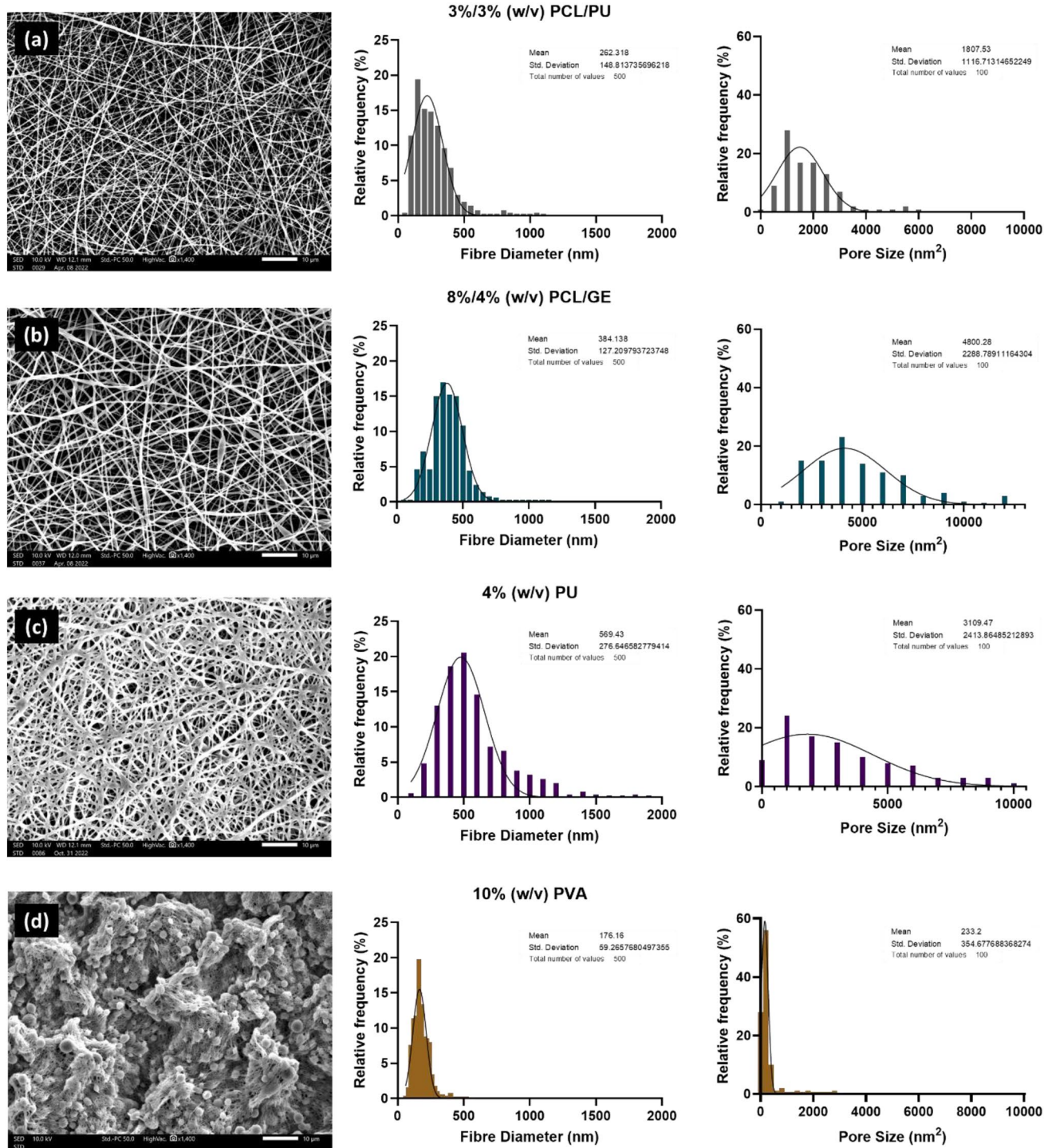


**Fig. 3** Morphology, fibre diameter and pore size distribution histograms. **(a)** SEM imaging example and frequency distribution histogram for fibre diameter ( $n=500$ ) and pore size ( $n=100$ ) of 5 replicates for 3%/3% (w/v) PCL/PU; **(b)** SEM imaging example and frequency distribution histogram for fibre diameter ( $n=500$ ) and pore size ( $n=100$ ) of 5 replicates for 8%/4% (w/v) PCL/Ge; **(c)** SEM imaging example and frequency distribution histogram for fibre diameter ( $n=500$ ) and pore size ( $n=100$ ) of 5 replicates for 4% (w/v) PU; **(d)** SEM imaging example and frequency distribution histogram for fibre diameter ( $n=500$ ) and pore size ( $n=100$ ) of 5 replicates for 10% (w/v) PVA. Scale bar is 10  $\mu\text{m}$  for SEM images

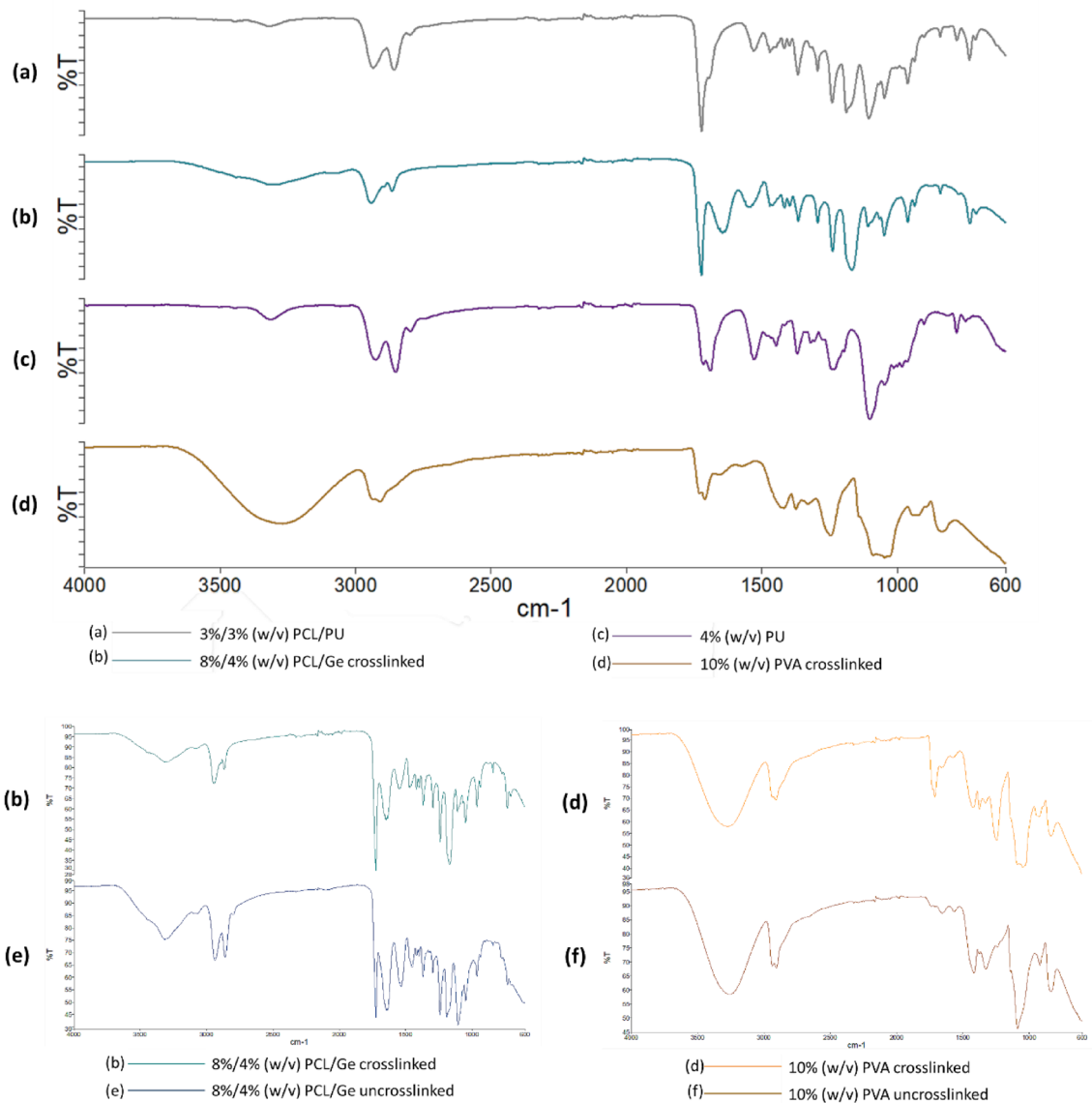


**Fig. 4** ATR-FTIR spectra for (a) 3%/3% (w/v) PCL/PU, (b) 8%/4% (w/v) PCL/Ge crosslinked, (c) 4% (w/v) PU, (d) 10% (w/v) PVA crosslinked, (e) 8%/4% (w/v) PCL/Ge uncrosslinked and (f) 10% (w/v) PVA uncrosslinked

angle of  $43.73 \pm 1.65^\circ$ . PVA-derived membranes have registered the lowest contact angle with  $31.96 \pm 5.83^\circ$ , but higher deviation in between samples.

### 3.4 Morphology and degradation rate

To evaluate the degradation rate of each of the samples, different parameters were assessed, such as pH, weight loss percentage and the modification of the surface morphology. None of the samples registered significant differences in pH when compared with the PBS control ( $\text{pH} = 6.36 \pm 0.02$ ) over the period of 15 days (Fig. 6 (1)). A slight variation of the pH was recorded at 30 days when comparing the samples with the PBS control ( $\text{pH} = 6.58 \pm 0.07$ ). The triplicates of 10% PVA registered a pH on the higher end of  $6.65 \pm 0.09$ . On the other hand, 3%/3% PCL/PU recorded a pH reading of  $6.45 \pm 0.02$ . 8%/4% PCL/Ge and 4% PU scaffold membranes recorded similar pH values of  $6.51 \pm 0.02$  and  $6.51 \pm 0.01$  respectively.

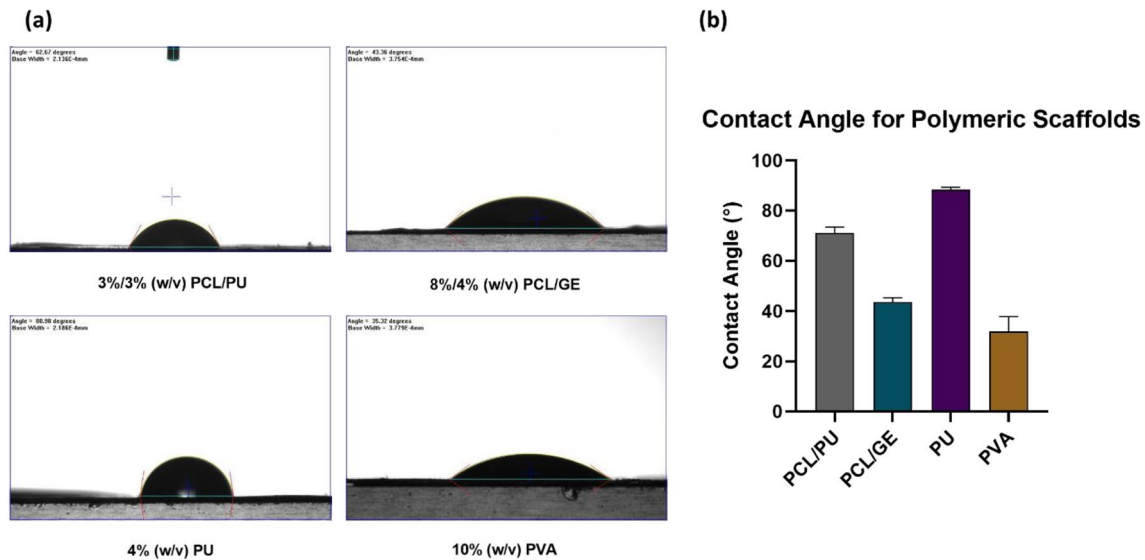


**Fig. 5** Contact angle measurements. **a** image of water droplet (1 $\mu$ L) morphology on four electrospun membranes with different compositions at 5 s; **b** contact angle results represented by their mean values with standard error bars of triplicates

Investigating the weight loss percentage recorded in Fig. 6. (2), all the samples recorded a loss of up to 10% of their weight over the 30-day period, confirming the degradation and modification of the scaffolds' surface. PCL/GE had the highest loss of  $8.97 \pm 1.83\%$  during the experimentation time, followed by 3%/3% PCL/PU with  $5.49 \pm 3.56\%$ , 10% PVA with  $4.67 \pm 1.55\%$  and finally 4% PU with a recorded loss of  $2.67 \pm 1.71\%$  of its weight.

All the samples recorded morphology changes after a 30-day period, including fibre breakage and shrinkage of the overall surface. Round structures were found in PCL-derived scaffolds, that could be derived from the degradation of the material, however, further studies would be necessary. As shown in Fig. 6 (3d), the 10% PVA scaffold changed significantly over the 30-day period, with significant shrinkage, fibre deformation and degradation of the folding structures into a flatter morphology. As predicted by the decreased weight loss in Fig. 6 (2), 4% PU is the scaffold with the least modified surface besides minor shrinkage of the pore size, suggesting that this scaffold provides further support and stability than the other candidate materials.

### 3.5 Mechanical tensile testing

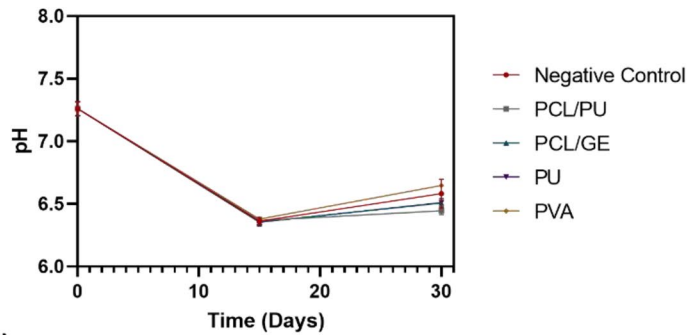
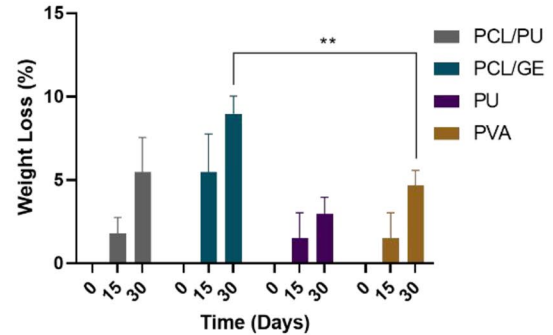
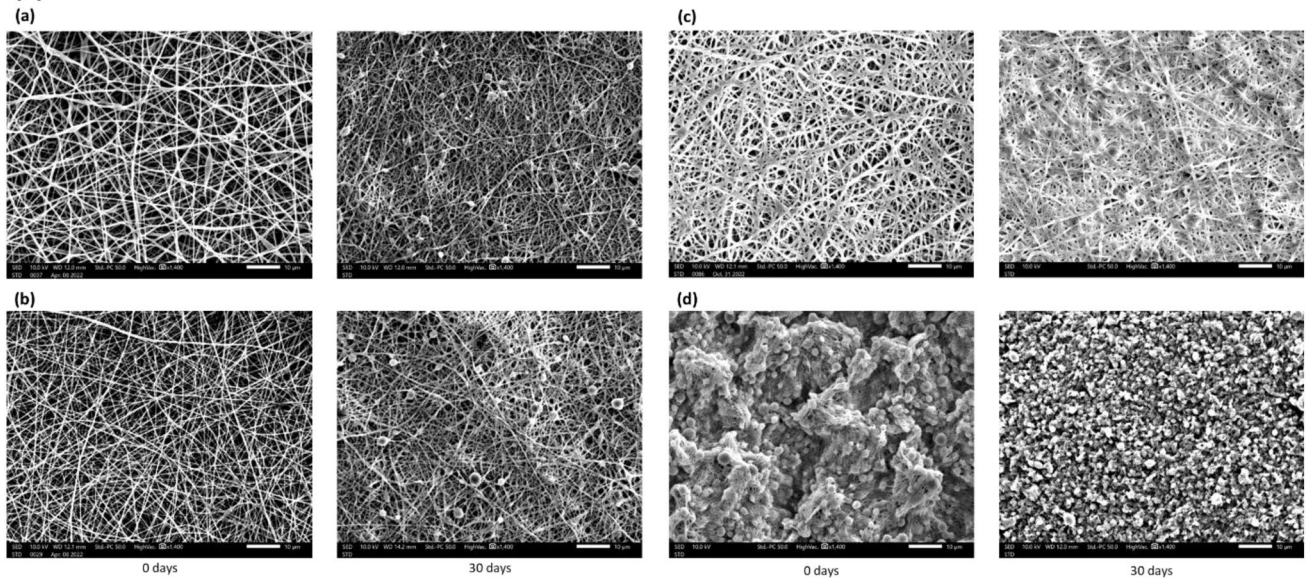
A tensile strength test was performed to analyse the mechanical behaviour of the electrospun scaffold samples by plotting the stress-strain curves. Results demonstrate that the blend of PCL has an impact on the mechanical stability of the scaffolds decreasing the Young Modulus from 0.38 MPa (4% PU) to 0.29 MPa (3%/3% PCL/PU) (see Fig. 7; and summary in Table 2). 8%/4% PCL/Ge measure the highest Young Modulus of the different candidates at 3.40 MPa and with only a 5.15 mm extension at the rupture point, followed by 10% PVA with a Young's Modulus of 1.91 MPa and 9.12 mm extension.

Scaffolds made of PU composition were revealed to have higher elasticity when compared with other materials, being able to extend with the range of 16.66 to 22.43 mm depending on the composition conjugate. The 10% PVA scaffold registered the highest tensile strength value of all the candidates at 0.85 MPa, followed by the 3%/3% PCL/PU at 0.27 MPa.

### 3.6 Cell proliferation assay

The membranes were then thoroughly washed in baths of ethanol and deionised water to remove any harsh solvents, followed by UV exposure for 30 min to guarantee sterilised conditions before cell seeding. To test the initial viability of the scaffolds, cells were seeded into these scaffolds with successful cellular proliferation and viability.

The proliferation rate of the HMF on the respective polymeric scaffolds was assessed via MTT assay (Fig. 8) and analysed with a 2-way ANOVA. After 3 days of incubation, the proliferation rate of the HMF cells was revealed to be similar or higher in most of the electrospun polymeric scaffolds (128% for 3%/3% PCL/PU, 55% for 8%/4% PCL/Ge, 119% for 4% PU, and 58% for 10% PVA) when compared with the Matrigel™, showing a mean of 49%. Longer periods of incubation

**(1) Degradation Rate of Polymeric Scaffolds****(2) Weight Loss over Time****(3)**

**Fig. 6** Degradation studies. (1) Graph representing pH variation over 30 day period for each of the electrospun samples, the results are represented by the mean of three replicates with standard error bars; (2) Weight loss percentage change over 30 days, results were analysed by a 2-way ANOVA with Tukey's multiple comparison test and represented by the means of three replicates and standard error bars with \* indicating significant differences between groups (\*\* $p < 0.01$ ); (3) Surface morphology imaging using SEM microscopy at beginning of degradation studies and after 30 days—**a** 3%/3% PCL/PU scaffolds morphology at 0 and 30 days; **b** 8%/4% PCL/Ge morphology at 0 and 30 days; **c** 4% PU scaffolds morphology at 0 and 30 days; **d** 10% PVA scaffolds morphology at 0 and 30 days. Scale bar is 10  $\mu\text{m}$  for SEM images

revealed that the electrospun polymeric scaffolds promoted higher proliferation rates when compared with the Matrigel™ condition. It is worth noting that after the incubation of these cells over the period of a week, the scaffolds composed of 3%/3% PCL/PU, 4% PU and 10% PVA showed almost twice as high percentages of cell growth, 252%, 184% and 158%, respectively, when compared to Matrigel™ condition at 100%. On the other hand, scaffolds composed of 8%/4% PCL/Ge registered slower proliferation and of cell growth, with a growth of 55% to 61% between 72 and 168 h, when compared with the other scaffold types.

### 3.7 Cellular morphology

Microscopic imaging was undertaken after a week incubation period to understand the HMF's morphologic behaviour in each of the scaffolds versus the control in Matrigel™ in order to select the best alternative (Fig. 9). Both 3%/3% PCL/PU and 8%/4% PCL/Ge scaffolds did not appear to stimulate cellular aggregation nor spheroid formation as demonstrated in Matrigel™. This morphological behaviour of the HMF is recurrent in membranes with larger pore sizes (1800–4800  $\text{nm}^2$  according to the mean represented in Fig. 3a and b), this could suggest cell penetration and migration within the scaffold itself [54]. 8%/4% PCL/Ge revealed some background fluorescence that can be attributed to the non-specific

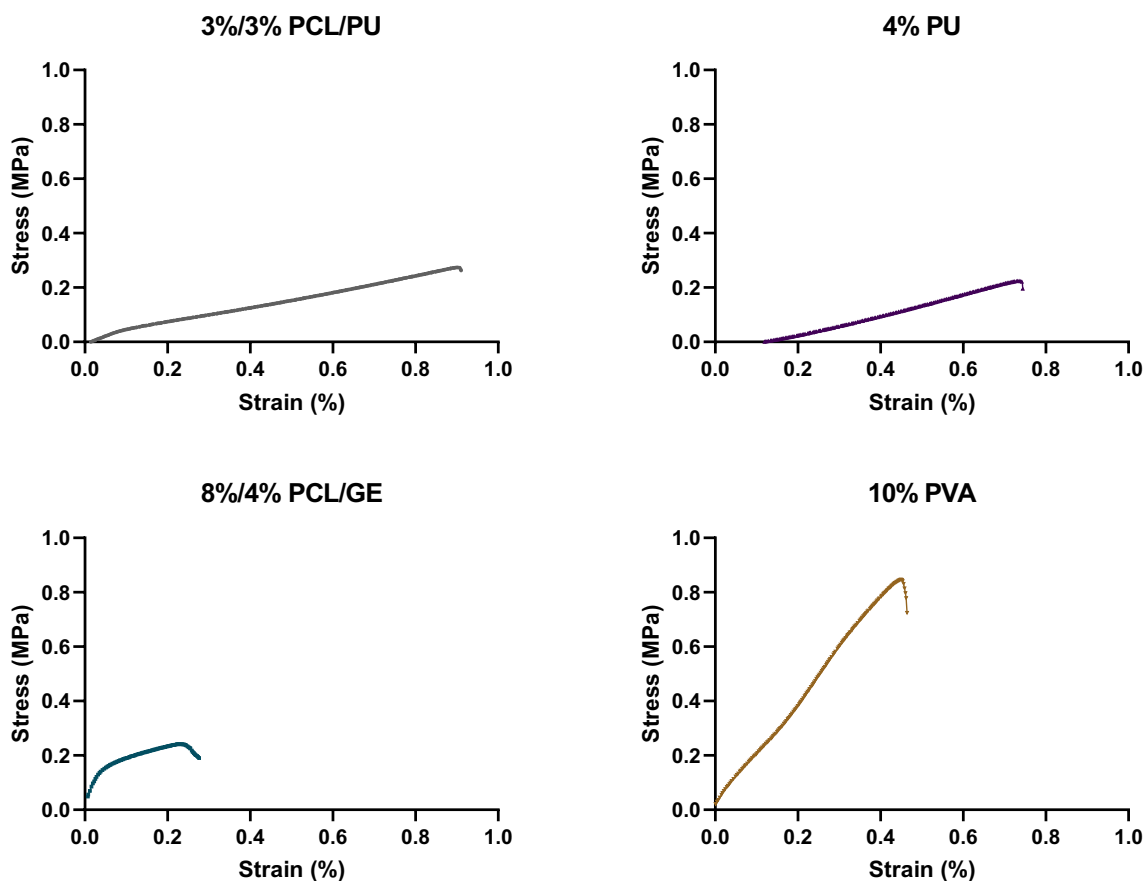


**Fig. 7** Stress–strain curve of various types of scaffolds. Tensile testing was carried out on 3%/3% (w/v) PCL/PU and 8%/4% (w/v) (PCL/Ge) composite scaffolds; 4% (w/v) PU and 10% (w/v) PVA and plotted in a stress–strain curve

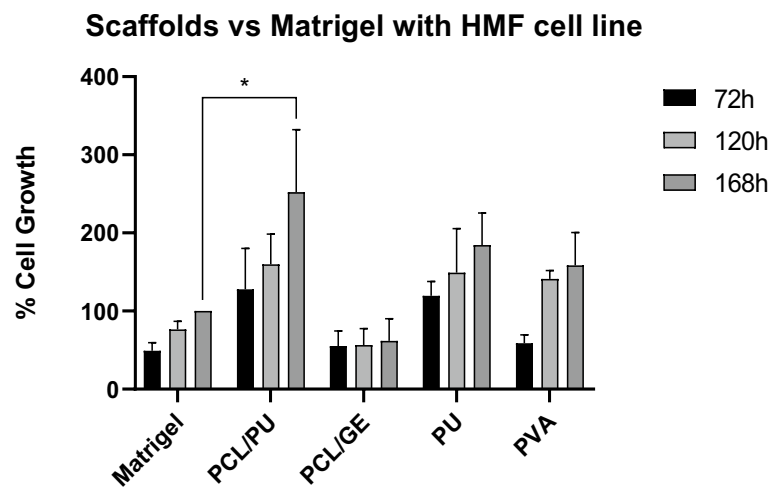
**Table 2** Tensile Strength properties of each electrospun scaffold

Sample Name	Length (mm)	Thickness (mm)	Width (mm)	Temperature (°C)	Tensile strength (MPa)	Elongation at break (mm)	Young modulus (MPa)
3%/3% PCL/PU	20	0.416	10	22	0.27	22.43	0.29
8%/4% PCL/Ge	20	0.358	10	20	0.24	5.15	3.40
4% PU	20	0.173	10	20	0.22	16.66	0.38
10% PVA	20	0.180	10	21	0.85	9.12	1.91

phalloidin binding to high concentrations of amino acids derived from the gelatin that is also found in the composition of actin filaments [55, 56].

Even though, there is a noteworthy decrease in the overall HMF cluster area size (Fig. 10) when comparing Matrigel™ (result mean of 116,436 μm<sup>2</sup>) to PU (result mean of 28,576 μm<sup>2</sup>) and PVA (mean area of 11,806 μm<sup>2</sup>). Both 3% PU and 10% PVA candidates demonstrate clustering formation similar to that which occurs in the Matrigel™ sample. The quantification of cluster size was performed using ImageJ software where the area of a total of 5 clusters was measured per condition. The figure below compares the mean ± standard error area sizes of the HMF clusters in Matrigel™, 4% PU and 10% PVA scaffolds. Nevertheless, 10% PVA-grown HMF clusters reorganised and grew with higher frequency (Fig. 9 (e1)) and smaller standard error between replicates when compared with its counterpart 4% PU (Figs. 9 (d1) and Fig. 10). A one sample t test was performed on the data represented in Fig. 8 with no statistical significance found.

**Fig. 8** MTT assay of HMF cellular proliferation rate in each of the polymeric candidates for 72 h, 120 h and 168 h timepoints. Values represent the means  $\pm$  standard error of the results from triplicates assays (N = 3) versus the control in Matrigel™. A 2-way ANOVA with Dunnett's multiple comparison test was performed comparing the scaffolds versus Matrigel™ with \* indicating significant differences between the groups (\* $p < 0.05$ )



## 4 Discussion

More than ever, there is an increasing need for well-characterised scaffolds, using manufacturing approaches that can be replicated within different research settings which are cost-efficient. Biocompatibility and cell toxicity were considered when selecting both the materials and solvents used for each of the electrospun membranes. The most commonly used solvents for PU electrospinning include DMF and THF due to their high dielectric property which results in less bead formation [57]. Nonetheless, these are associated with growth inhibitory effects, for example, in breast epithelial cell lines, such as MCF-12A [58]. Attempts to produce nanofibrous scaffolds with decreased cell toxicity using solvents reported in literature, such as, chloroform/methanol, deionised water (DI) and TFE were used in this study to address this issue [59, 60]. The solution mixtures were then assessed on their ability to be electrospun and the parameters used were optimised until improved samples with low/no beading were achieved. Increased mean fibre diameter is known to contribute to cell intravasation and proliferation, due to the facilitation of nutrient transport and oxygen within in vitro conditions [61]. 4% PU derived scaffolds registered the highest fibre diameter and 8%/4% PCL/Ge demonstrated the highest pore size. Even though, both of these scaffolds demonstrated high proliferation rates of HMF, the cellular organisation distinctly diverged with the PCL/Ge scaffolds allowing for cell infiltration due to the higher pore size. These findings are supported by Lowery, J. et al., study, where dermal fibroblasts thrived in higher pore size electrospun scaffolds [62] showing that pore size is crucial for cell migration and fibre diameter enhances the surface area for cells to adhere. The manipulation of fibres diameter can be achieved by a variety of parameters change such as, the reduction of voltage and elongation of the fibres and by adding polymers like PCL that have a direct impact on the scaffold morphology demonstrated in the comparison between PU and PCL/PU composite scaffolds. Moreover, studies have shown that the solvent permittivity can be used to manipulate fibre morphology, with the polarity of these reagents playing a critical role in size and crystallinity of the formed fibres. A study conducted by Ambrosio et al., has shown that polymeric solutions of PCL with solvents of higher dielectric constant tend to form reduced size diameter fibres [60]. In this study, 4% PU scaffold showed fibres with a diameter double the width compared to 3%/3% PCL/PU scaffolds and higher than 8%/4% PCL/Ge, this may be a result of the use of methanol ( $\epsilon = 32.7$ )/chloroform ( $\epsilon = 4.81$ ) [63] solvent solution in 4% PU scaffolds versus the TFE ( $\epsilon = 27$ ) used in PCL and PU composite materials [64]. Comparing to the other counterparts, scaffolds derived from 10% PVA demonstrated higher batch variability with decreased quality of nanofibres. We hypothesise that the lack of consistency may result from the absence of temperature and humidity control in our electrospinning setup. These parameters have been proven to be crucial for the electrospinning of PVA polymeric solutions, such as the decreasing of fibre diameter with reduced humidities [65, 66]. This resulted on the electrospaying of the PVA polymeric solution onto the collector plate [67]. Even though this material did not produce the expected type of membrane, HMF viability studies demonstrated high proliferation rate and organotypic organisation.

[54] Once morphology of the fibres was assessed, FT-IR was used as a rapid characterisation of the functional group of each of the polymers. The infrared spectra of each of the scaffold demonstrated that the different polymers (Ge and

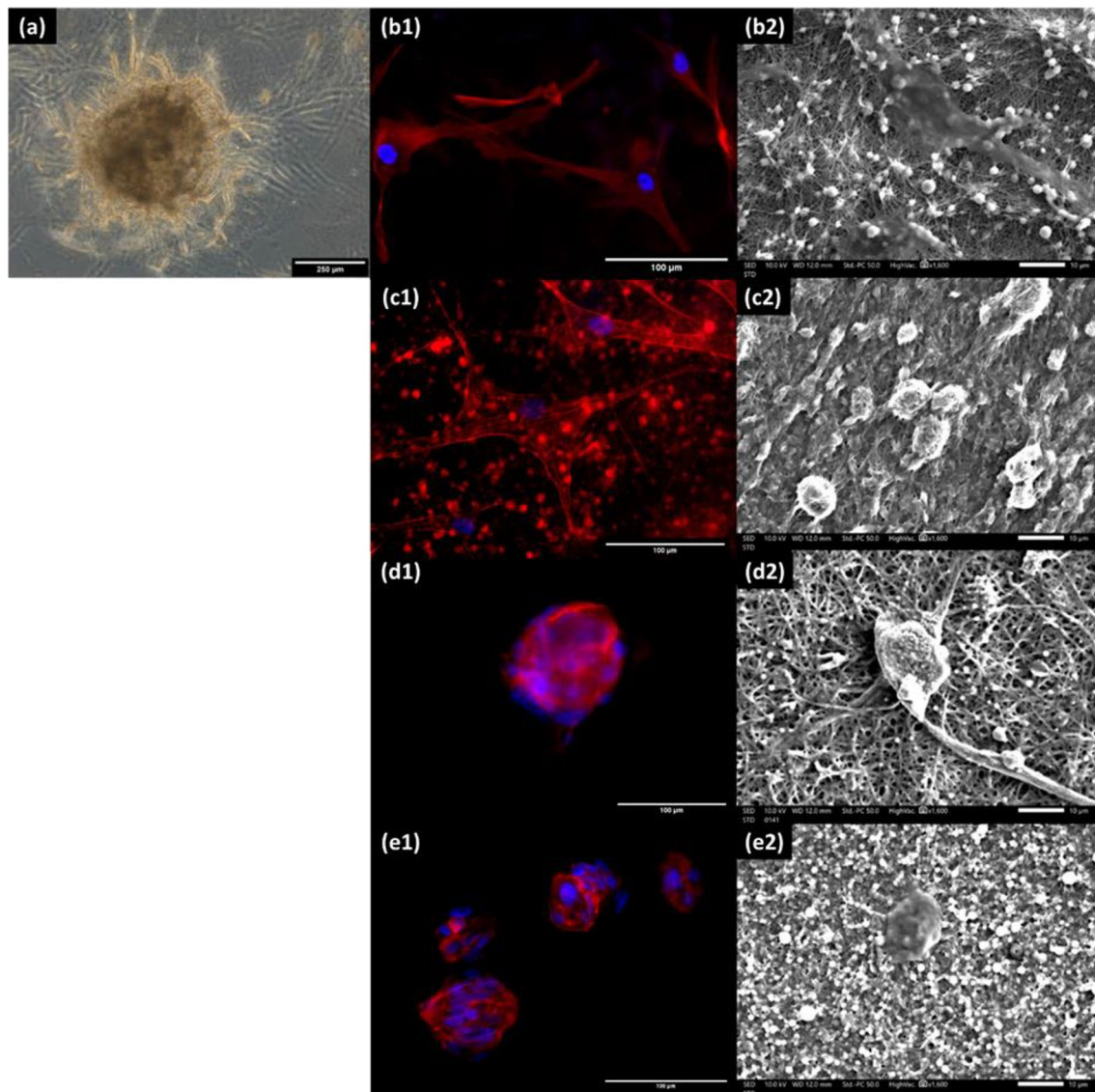
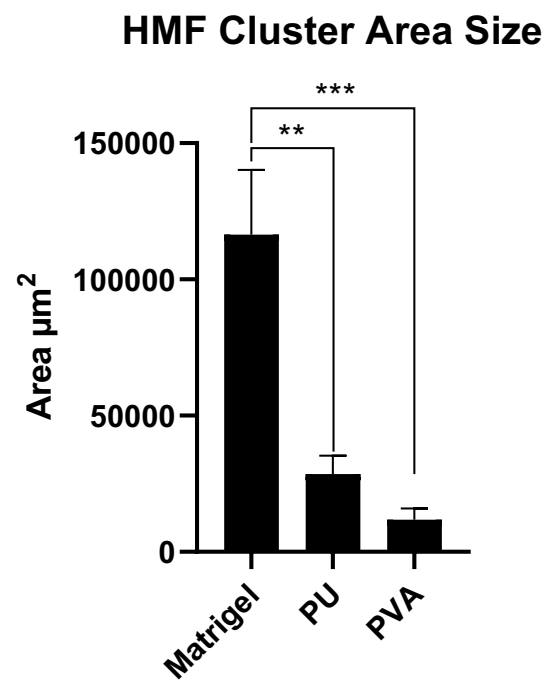


**Fig. 9** HMF morphology after 1 week (168 h) incubation period in the different polymeric scaffolds versus Matrigel™ **a** Light microscopy of HMF clusters incubated for 1 week in Matrigel™ (control) at magnification 10x; **(b1 to e1)** Imaging of HMF morphology in the different scaffolds after 1 week incubation—fluorescence microscopy (centre) with DAPI staining for nuclei (blue) and Alexa Fluor™ 594 Phalloidin staining for actin filaments (red) at 20× magnification; **(b2 to e2)** SEM Microscopy imaging of surface interactions between the different candidates and HMF cells at ×1600 magnification (right); **(b1 and b2)** HMF seeded in 3%/3% PCL/PU scaffolds; **(c1 and c2)** HMF seeded in 8%/4% PCL/Ge scaffolds; **(d1 and d2)** HMF seeded in 4% PU scaffolds; **(e1 and e2)** HMF seeded in 10% PVA scaffolds. Scale bar is 10 μm for SEM images

PU) were successfully conjugated within the PCL blends, by exhibiting peaks that are not found in PCL scaffolds, such as, Amide groups I, II and A [51, 68, 69].

Due to PVA and Gelatin being soluble in a water-based solution, the composite scaffolds underwent a process of crosslinking that aimed to form stable covalent bonds between the different polymers, thus avoiding rapid degradation in cell culturing conditions [70, 71]. The 10% (w/v) PVA samples were stabilised using a thermal crosslinking, this process was chosen as the optimal technique to prevent the use of further harmful chemicals. This type of crosslinking method has been used to obtain stabilised PVA membranes for a variety of biomedical application since thermal crosslinking reduces the degree of swelling in these scaffold [66]. According to FT-IR results, the stability of the fibres via heat exposure did not shift the peaks displayed in PVA-derived membranes when comparing crosslinked with uncrosslinked samples. Nonetheless, there is an increased intensity in uncrosslinked samples suggesting fewer bonds and consequently higher

**Fig. 10** HMF cluster area size comparison between incubation conditions. Values represent the means  $\pm$  standard error of the results from 5 different spheroids grown in the scaffold versus the control in Matrigel™ grown for a period of 7 days (N=2). A one-way ANOVA with Dunnett's multiple comparison test was performed comparing the scaffolds versus Matrigel™ with \* indicating significant differences from the Matrigel™ control group (\* $p < 0.05$ , \*\* $p < 0.01$ , \*\*\* $p < 0.001$ )



instability of the fibres. Similar results are observed in Ge composite scaffolds, which were crosslinked chemically, using Glutaraldehyde. Even though literature reports other methods, that have a smaller cytotoxic impact, glutaraldehyde was selected due to reagent availability [72]. Wettability surface properties were studied to assess the hydrophilicity of each scaffold as a proxy for cell attachment and healthy cellular behaviour. PCL is a naturally hydrophobic with a contact angle at around  $140^\circ$ , and as such is often conjugated with other polymers to improve wettability values and cell attachment [73]. Our PCL blends register contact angles below  $90^\circ$  for Ge and PU conjugates indicating good wettability score for cell seeding. As expected, PVA scaffolds display the higher hydrophilic behaviour of all the candidates with a contact angle around  $32^\circ$ . These results fall within the range suitable for cell attachment ( $5^\circ$ - $150^\circ$ ) [74].

Scaffolds must be able to tune to their cellular microenvironment and, as such, are required to provide stability but not compete with newly formed tissue. This can be achieved by allowing a controlled degradation of the membranes by synchronising the polymer degradation with the replacement of the natural ECM [75]. The degradation rate of each scaffold was measured in terms of weight loss, pH changes and morphology changes. Compared to the negative control (PBS), representative of the physiological environment, the samples' pH remained around the expected values of 6.6, suggesting that degradation byproducts do not affect the medium and a viable pH for cellular growth (6.5–10.5) is maintained [76]. The weight loss analysis confirmed that the scaffolds are able to sustain cellular growth for long periods with only 10% weight loss for all the recorded samples. Moreover, when performing SEM imaging after 30 days, images confirmed significant shrinkage and surface architecture degradation of all the samples.

The combination of hydrophobic material but mechanically sound like PCL with PU and Ge, known for their biocompatible properties, creates scaffolds with enhanced ability to support tissue growth. To investigate this, tensile strength tests were undertaken to characterise the strength and elasticity modulus of each sample. The addition of PCL to the composite blends significantly increased the mechanical stability of the PU scaffold increasing its elongation from 183 to 212.15%. Each of the scaffolds was shown to have different properties with 8%/4% (w/v) PCL/Ge being the stiffer membrane, followed by 10% (w/v) PVA suggesting that these scaffolds would be adequate for the growth of tissue like cartilage [77]. PVA-derived membranes also had a higher tensile strength at 0.85 MPa, proving this membrane had the ability to withstand higher loads compared to the other types. Characteristics such as mechanical forces and the stability of a scaffold have been proven to stimulate cell proliferation and are key to emulating physical cues in vitro models such as peristaltic movements. Moreover, stiffness has been identified as a highly potent regulator of cell differentiation and migration [78].

Cellular adhesion provides an insight into how cell behaviour is affected by scaffold properties such as surface and chemistry. Fluorescence staining and SEM imaging allow for the observation of cellular attachment and morphological

behaviour within the substrate to which it was seeded. The HMF seeded in the Matrigel™ (control) demonstrated the formation of clusters with sparse outgrowth at the extremities. This behaviour was only observed in two other electrospun membranes, 4% PU and 10% PVA. Even though literature suggests the formation of cellular spheroids when HMF are co-culture with epithelial cell lines (e.g. MCF-7S1), there is very little available data regarding the behaviour of HMF single cultures in Matrigel™ [79]. These results demonstrated notably smaller area sizes in the electrospun scaffolds versus the control. It is worth noting that even though PU generated clusters twice the size as the ones observed in PVA conditions, PVA induced had a higher frequency of cluster formation. Interestingly, the beaded architecture of PVA membranes appeared to increase the points of attachment for cells to adhere despite the formation of beads during the electrospinning process often being considered undesirable due to the lack of uniformity through the scaffold surface [44, 80].

All the scaffold candidates, except the PCL/Ge composite membranes, presented substantially higher proliferation rates than the Matrigel™ control. This could be a result of the bigger fibre and diameter size that change surface morphology, emulating the native ECM fibrillary structure [81]. Nonetheless, further studies need to be conducted to assess the effect that these densely compacted nanofibres have on cell infiltration to further optimise proliferation and behaviour. [82].

## 5 Conclusion

The aim of the present work was to explore the manufacture of three-dimensional synthetic electrospun scaffolds that could be used for the growth of breast organotypic tissues, by selecting techniques that use less harsh solvents, when possible, without affecting the quality of the membrane manufactured. This feasibility study demonstrated, for the first time, that HMF proliferation can be supported by electrospun scaffolds and even emulate cell reorganisation in Matrigel™ to a certain extent, and the potential it has to replace this hydrogel in other breast derived tissues. In this study we highlight the role surface characteristics play in cell morphology and and organisation. Fibroblasts grown on electrospun membranes with smaller pore and fiber diameter sizes reorganised in a closer manner to those observed in the control and exhibited higher proliferation rates. It concluded that scaffold characterisation, optimisation of scaffold manufacturing techniques and materials is a powerful tool to bridge the gap of standardisation. Our results should contribute to the creation of scaffolds centred around tissue growth applications that could be used by other research groups for the growth of a variety of in vitro models. Nevertheless, further studies should be undertaken to further tailor the tunability of these scaffolds fore breast tissue growth.

**Acknowledgements** All experiments were conducted in the Organ-on-a-Chip Research and Tissue Culture laboratories of Brunel University London. The authors would like to express their gratitude to EPSRC, UKRI and Breast Cancer UK for the financial support provided. We are deeply thankful to Dr Aya Aly for her invaluable advice and insightful comments, which greatly improved the quality of this manuscript.

**Author contributions** Conceptualisation, L.A.O., R.E.M., and E.S.; literature assessment, L.A.O.; experimental design, L.A.O., A.N; results acquisition and analysis, L.A.O.; writing—original draft preparation, L.A.O.; writing—review and editing, L.A.O., A.A., R.E.M., and E.S. All authors have read and agreed to the published version of the manuscript.

**Funding** This work was supported by an Engineering and Physical Sciences Research Council (EPSRC) Doctoral Training Programme Studentship and a research grant from Breast Cancer UK (BCUK).

**Data availability** Data sets generated during the current study are available from the corresponding author on reasonable request.

## Declarations

**Ethics approval and consent to participate** Not applicable.

**Consent for publication** All the involved parties have given their consent for this publication.

**Competing interests** The authors have no relevant financial or non-financial interests to disclose.

**Open Access** This article is licensed under a Creative Commons Attribution 4.0 International License, which permits use, sharing, adaptation, distribution and reproduction in any medium or format, as long as you give appropriate credit to the original author(s) and the source, provide a link to the Creative Commons licence, and indicate if changes were made. The images or other third party material in this article are included in the article's Creative Commons licence, unless indicated otherwise in a credit line to the material. If material is not included in the article's Creative Commons licence and your intended use is not permitted by statutory regulation or exceeds the permitted use, you will need to obtain permission directly from the copyright holder. To view a copy of this licence, visit <http://creativecommons.org/licenses/by/4.0/>.

## References

1. Polyak K, Kalluri R. The role of the microenvironment in mammary gland development and cancer. *Cold Spring Harb Perspect Biol.* 2010;2:a003244–a003244. <https://doi.org/10.1101/cshperspect.a003244>.
2. Engel A, Frenzel F, Niemann B, Braeuning A, Lampen A, Buhrke T. The use of 3D cultures of MCF-10A and MCF-12A cells by high content screening for effect-based analysis of non-genotoxic carcinogens. *Toxicol In Vitro.* 2019;59:55–63. <https://doi.org/10.1016/j.tiv.2019.04.008>.
3. Quail DF, Joyce JA. Microenvironmental regulation of tumor progression and metastasis. *Nat Med.* 2013;19:1423–37. <https://doi.org/10.1038/nm.3394>.
4. DeCosse JJ, Gossens C, Kuzma JF, Unsworth BR. Embryonic inductive tissues that cause histologic differentiation of murine mammary carcinoma in vitro. *J Natl Cancer Inst.* 1975;54:913–22.
5. Yamazaki K, Eyden BP. Characterisation of breast stromal fibroblasts: Cell surface distribution of collagen type IV, laminin and fibronectin. *J Submicrosc Cytol Pathol.* 1998;30:217–26.
6. Plikus MV, Wang X, Sinha S, Forte E, Thompson SM, Herzog EL, Driskell RR, Rosenthal N, Biernaskie J, Horsley V. Fibroblasts: origins, definitions, and functions in health and disease. *Cell.* 2021;184:3852–72. <https://doi.org/10.1016/j.cell.2021.06.024>.
7. Bhowmick NA, Neilson EG, Moses HL. Stromal fibroblasts in cancer initiation and progression. *Nature.* 2004;432:332–7. <https://doi.org/10.1038/nature03096>.
8. Avagliano A, Fiume G, Ruocco MR, Martucci N, Vecchio E, Insabato L, Russo D, Accurso A, Masone S, Montagnani S, et al. Influence of fibroblasts on mammary gland development, breast cancer microenvironment remodeling, and cancer cell dissemination. *Cancers (Basel).* 2020;12:1697. <https://doi.org/10.3390/cancers12061697>.
9. Ao Z, Shah SH, Machlin LM, Parajuli R, Miller PC, Rawal S, Williams AJ, Cote RJ, Lippman ME, Datar RH, et al. Identification of cancer-associated fibroblasts in circulating blood from patients with metastatic breast cancer. *Cancer Res.* 2015;75:4681–7. <https://doi.org/10.1158/0008-5472.CAN-15-1633>.
10. Kuperwasser C, Chavarría T, Wu M, Magrane G, Gray JW, Carey L, Richardson A, Weinberg RA. Reconstruction of functionally normal and malignant human breast tissues in mice. *Proc Natl Acad Sci.* 2004;101:4966–71. <https://doi.org/10.1073/pnas.0401064101>.
11. Shekhar MP, Werdell J, Santner SJ, Pauley RJ, Tait L. Breast Stroma plays a dominant regulatory role in breast epithelial growth and differentiation: implications for Tumor development and progression. *Cancer Res.* 2001;61:1320–6.
12. Phan-Lai V, Florczyk SJ, Kievit FM, Wang K, Gad E, Disis ML, Zhang M. Three-dimensional scaffolds to evaluate Tumor associated fibroblast-mediated suppression of breast Tumor specific T cells. *Biomacromol.* 2013;14:1330–7. <https://doi.org/10.1021/bm301928u>.
13. Wang X, Sun L, Maffini MV, Soto A, Sonnenschein C, Kaplan DL. A complex 3D human tissue culture system based on mammary stromal cells and silk scaffolds for modeling breast morphogenesis and function. *Biomaterials.* 2010;31:3920–9. <https://doi.org/10.1016/j.biomaterials.2010.01.118>.
14. Rijal G, Li W. 3D scaffolds in breast cancer research. *Biomaterials.* 2016;81:135–56. <https://doi.org/10.1016/j.biomaterials.2015.12.016>.
15. Kohane DS, Langer R. Polymeric biomaterials in tissue engineering. *Pediatr Res.* 2008;63:487–91. <https://doi.org/10.1203/01.pdr.0000305937.26105.e7>.
16. Merotto E, Pavan PG, Piccoli M. Three-dimensional bioprinting of naturally derived hydrogels for the production of biomimetic living tissues: benefits and challenges. *Biomedicines.* 2023;11:1742. <https://doi.org/10.3390/biomedicines11061742>.
17. Aisenbrey EA, Murphy WL. Synthetic alternatives to matrigel. *Nat Rev Mater.* 2020;5:539–51. <https://doi.org/10.1038/s41578-020-0199-8>.
18. Tsou Y-H, Khoneisser J, Huang P-C, Xu X. Hydrogel as a bioactive material to regulate stem cell fate. *Bioact Mater.* 2016;1:39–55. <https://doi.org/10.1016/j.bioactmat.2016.05.001>.
19. Osório LA, Silva E, Mackay RE. A review of biomaterials and scaffold fabrication for organ-on-a-chip (OOAC) systems. *Bioengineering.* 2021;8:113. <https://doi.org/10.3390/bioengineering8080113>.
20. Sabaté Rovira D, Nielsen HM, Taboryski R, Bunea A-I. Additive manufacturing of polymeric scaffolds for biomimetic cell membrane engineering. *Mater Des.* 2021;201:109486. <https://doi.org/10.1016/j.matdes.2021.109486>.
21. Wang N, Burugapalli K, Song W, Halls J, Moussy F, Zheng Y, Ma Y, Wu Z, Li K. Tailored fibro-porous structure of electrospun polyurethane membranes, their size-dependent properties and trans-membrane glucose diffusion. *J Memb Sci.* 2013;427:207–17. <https://doi.org/10.1016/j.memsci.2012.09.052>.
22. Liliana L, Aldo B. Electrospinning with benign solvents: feasibility study and versatile use of Poly(Epsilon-Caprolactone) fibers. *Front Bioeng Biotechnol.* 2016. <https://doi.org/10.3389/conf.FBIOE.2016.01.01826>.
23. Doustgani A, Vasheghani-Farahani E, Soleimani M, Hashemi-Najafabadi S. Optimizing the mechanical properties of electrospun polycaprolactone and nanohydroxyapatite composite nanofibers. *Compos B Eng.* 2012;43:1830–6. <https://doi.org/10.1016/j.compositesb.2012.01.051>.
24. Can-Herrera LA, Oliva AI, Dzul-Cervantes MAA, Pacheco-Salazar OF, Cervantes-Uc JM. Morphological and mechanical properties of electrospun polycaprolactone scaffolds: Effect of applied voltage. *Polymers (Basel).* 2021;13:662. <https://doi.org/10.3390/polym13040662>.
25. Chaudhari A, Vig K, Baganizi D, Sahu R, Dixit S, Dennis V, Singh S, Pillai S. Future prospects for scaffolding methods and biomaterials in skin tissue engineering: a review. *Int J Mol Sci.* 1974;2016:17. <https://doi.org/10.3390/ijms17121974>.
26. Wu S, Liu X, Yeung KWK, Liu C, Yang X. Biomimetic porous scaffolds for bone tissue engineering. *Mater Sci Eng R Rep.* 2014;80:1–36. <https://doi.org/10.1016/j.mser.2014.04.001>.
27. Perez-Puyana V, Jiménez-Rosado M, Romero A, Guerrero A. Polymer-based scaffolds for soft-tissue engineering. *Polymers (Basel).* 2020;12:1566. <https://doi.org/10.3390/polym12071566>.
28. Guo B, Ma PX. Synthetic biodegradable functional polymers for tissue engineering: a brief review. *Sci China Chem.* 2014;57:490–500. <https://doi.org/10.1007/s11426-014-5086-y>.
29. Christen M-O, Vercesi F. Polycaprolactone: How a well-known and futuristic polymer has become an innovative collagen-stimulator in esthetics. *Clin Cosmet Investig Dermatol.* 2020;13:31–48. <https://doi.org/10.2147/CCID.S229054>.

30. BSI. Knowledge Implants for Surgery. Homopolymers, Copolymers and Blends on Poly(Lactide). In Vitro Degradation Testing.
31. Yue H, Xie K, Ji X, Xu B, Wang C, Shi P. Vascularized neural constructs for ex-vivo reconstitution of blood-brain barrier function. *Biomaterials*. 2020;245: 119980. <https://doi.org/10.1016/j.biomaterials.2020.119980>.
32. Sousa I, Mendes A, Bártolo PJ. PCL scaffolds with collagen bioactivator for applications in tissue engineering. *Procedia Eng*. 2013;59:279–84. <https://doi.org/10.1016/j.proeng.2013.05.122>.
33. Zhan J, Lan P. The review on electrospun gelatin fiber scaffold. *J Res Updat Polym Sci*. 2012;1(2):59. <https://doi.org/10.6000/1929-5995.2012.01.02.1>.
34. Ramón-Azcón J, Ahadian S, Obregón R, Camci-Unal G, Ostrovidov S, Hosseini V, Kaji H, Ino K, Shiku H, Khademhosseini A, et al. Gelatin methacrylate as a promising hydrogel for 3D microscale organization and proliferation of dielectrophoretically patterned cells. *Lab Chip*. 2012;12:2959. <https://doi.org/10.1039/c2lc40213k>.
35. Yang L, Shridhar SV, Gerwitz M, Soman P. An in vitro vascular chip using 3d printing-enabled hydrogel casting. *Biofabrication*. 2016;8: 035015. <https://doi.org/10.1088/1758-5090/8/3/035015>.
36. El-Seedi HR, Said NS, Yosri N, Hawash HB, El-Sherif DM, Abouzid M, Abdel-Daim MM, Yaseen M, Omar H, Shou Q, et al. Gelatin nanofibers: recent insights in synthesis. *Bio-Med Appl Limit Heliyon*. 2023;9: e16228. <https://doi.org/10.1016/j.heliyon.2023.e16228>.
37. Hong, Y. Electrospun Fibrous Polyurethane Scaffolds in Tissue Engineering. In *Advances in Polyurethane Biomaterials*; Elsevier, 2016; pp. 543–559.
38. Teixeira MA, Amorim MTP, Felgueiras HP. Poly(Vinyl Alcohol)-based nanofibrous electrospun scaffolds for tissue engineering applications. *Polymers (Basel)*. 2019;12:7. <https://doi.org/10.3390/polym12010007>.
39. Gao X, Wen M, Liu Y, Hou T, Niu B, An M. Synthesis and characterization of PU/PLCL/CMCS electrospun scaffolds for skin tissue engineering. *Polymers (Basel)*. 2022;14:5029. <https://doi.org/10.3390/polym14225029>.
40. Badea MA, Balas M, Hermenean A, Ciceu A, Herman H, Ionita D, Dinischioti A. Influence of matrigel on single- and multiple-spheroid cultures in breast cancer research. *SLAS Discov*. 2019;24:563–78. <https://doi.org/10.1177/2472555219834698>.
41. Gil-Castell O, Badia JD, Ontoria-Oviedo I, Castellano D, Sepúlveda P, Ribes-Greus A. Polycaprolactone/gelatin-based scaffolds with tailored performance: In vitro and in vivo validation. *Mater Sci Eng: C*. 2020;107:110296. <https://doi.org/10.1016/j.msec.2019.110296>.
42. Zhuo H, Hu J, Chen S, Yeung L. Preparation of polyurethane nanofibers by electrospinning. *J Appl Polym Sci*. 2008;109:406–11. <https://doi.org/10.1002/app.28067>.
43. Khan K-H, Masroor S, Rizvi G. Electrospinning and electrospun based polyvinyl alcohol nanofibers utilized as filters and sensors in the real world. *J Polym Eng*. 2023;43:627–39. <https://doi.org/10.1515/polyeng-2023-0044>.
44. Haider A, Haider S, Kang I-K. A comprehensive review summarizing the effect of electrospinning parameters and potential applications of nanofibers in biomedical and biotechnology. *Arab J Chem*. 2018;11:1165–88. <https://doi.org/10.1016/j.arabjch.2015.11.015>.
45. Xue J, Wu T, Dai Y, Xia Y. Electrospinning and electrospun nanofibers: Methods, materials, and applications. *Chem Rev*. 2019;119:5298–415. <https://doi.org/10.1021/acs.chemrev.8b00593>.
46. Cipitria A, Skelton A, Dargaville TR, Dalton PD, Huttmacher DW. Design, fabrication and characterization of pcl electrospun scaffolds—a review. *J Mater Chem*. 2011;21:9419–53. <https://doi.org/10.1039/c0jm04502k>.
47. Avossa J, Herwig G, Toncelli C, Itel F, Rossi RM. Electrospinning based on benign solvents: Current definitions. *Implic Strateg Green Chem*. 2022;24:2347–75. <https://doi.org/10.1039/D1GC04252A>.
48. Jia W, Li M, Weng H, Gu G, Chen Z. Design and comprehensive assessment of a biomimetic tri-layer tubular scaffold via biodegradable polymers for vascular tissue engineering applications. *Mater Sci Eng, C*. 2020;110: 110717. <https://doi.org/10.1016/j.msec.2020.110717>.
49. Abdal-hay A, Bartnikowski M, Hamlet S, Ivanovski S. Electrospun biphasic tubular scaffold with enhanced mechanical properties for vascular tissue engineering. *Mater Sci Eng, C*. 2018;82:10–8. <https://doi.org/10.1016/j.msec.2017.08.041>.
50. Cruz-Maya I, Varesano A, Vineis C, Guarino V. Comparative study on protein-rich electrospun fibers for in vitro applications. *Polymers (Basel)*. 2020;12:1671. <https://doi.org/10.3390/polym12081671>.
51. Chong LH, Lim MM, Sultana N. Fabrication and evaluation of polycaprolactone/gelatin-based electrospun nanofibers with antibacterial properties. *J Nanomater*. 2015;2015:1–8. <https://doi.org/10.1155/2015/970542>.
52. Kuppan P, Sethuraman S, Krishnan UM. PCL and PCL-gelatin nanofibers as esophageal tissue scaffolds: optimization, characterization and cell-matrix interactions. *J Biomed Nanotechnol*. 2013;9:1540–55. <https://doi.org/10.1166/jbn.2013.1653>.
53. Alwan TJ, Toma ZA, Kudhier MA, Ziadan KM. Preparation and characterization of the PVA nanofibers produced by electrospinning. *Madridge J Nanotechnol Nanosci*. 2016;1:1–3.
54. Ameer JM, Pr AK, Kasoju N. Strategies to tune electrospun scaffold porosity for effective cell response in tissue engineering. *J Funct Biomater*. 2019;10(3):30. <https://doi.org/10.3390/jfb10030030>.
55. Lee CH, Chin KB. Evaluation of pork myofibrillar protein gel with pork skin gelatin on rheological properties at different salt concentrations. *Food Sci Anim Resour*. 2019;39:576–84. <https://doi.org/10.5851/kosfa.2019.e48>.
56. Barthes J, Mutschler A, Dollinger C, Gaudinat G, Lavalle P, Le Houerou V, Brian McGuinness G, Engin Vrana N. Establishing contact between cell-laden hydrogels and metallic implants with a biomimetic adhesive for cell therapy supported implants. *Biomed Mater*. 2017;13: 015015. <https://doi.org/10.1088/1748-605X/aa895b>.
57. Akduman, C., Kumbasar, E.P.A. Electrospun Polyurethane Nanofibers. In *Aspects of Polyurethanes*; InTech, 2017.
58. Zhang J, Zhou D, Zhang L, Lin Q, Ren W, Zhang J, Nadeem L, Xu G. Dual effects of N, N-dimethylformamide on cell proliferation and apoptosis in breast cancer. Dose-Response. 2017;15:155932581774445. <https://doi.org/10.1177/1559325817744450>.
59. Lohmann R, Cousins IT, DeWitt JC, Glüge J, Goldenman G, Herzke D, Lindstrom AB, Miller MF, Ng CA, Patton S, et al. Are fluoropolymers really of low concern for human and environmental health and separate from other PFAS? *Environ Sci Technol*. 2020;54:12820–8. <https://doi.org/10.1021/acs.est.0c03244>.
60. Podgórski R, Wojsiński M, Ciach T. Nanofibrous materials affect the reaction of cytotoxicity assays. *Sci Rep*. 2022;12:9047. <https://doi.org/10.1038/s41598-022-13002-w>.
61. Loh QL, Choong C. Three-dimensional scaffolds for tissue engineering applications: role of porosity and pore size. *Tissue Eng Part B Rev*. 2013;19:485–502. <https://doi.org/10.1089/ten.teb.2012.0437>.

62. Lowery JL, Datta N, Rutledge GC. Effect of fiber diameter, pore size and seeding method on growth of human dermal fibroblasts in electrospun poly( $\epsilon$ -Caprolactone) fibrous mats. *Biomaterials*. 2010;31:491–504. <https://doi.org/10.1016/j.biomaterials.2009.09.072>.
63. Guarino V, Cirillo V, Taddei P, Alvarez-Perez MA, Ambrosio L. Tuning size scale and crystallinity of PCL electrospun fibres via solvent permissibility to address HMSC response. *Macromol Biosci*. 2011;11:1694–705. <https://doi.org/10.1002/mabi.201100204>.
64. Morrelli D, Guerra JG, Kumar P, Bajwa B, Krishnan VV, Maitra S. Role of solvent dielectric constant on the enthalpy-entropy compensation in the hindered amide bond rotation. *Chem Phys Lett*. 2022;792: 139412. <https://doi.org/10.1016/j.cplett.2022.139412>.
65. Raksa A, Numpaisal P, Ruksakulpiwat Y. The effect of humidity during electrospinning on morphology and mechanical properties of SF/PVA nanofibers. *Mater Today Proc*. 2021;47:3458–61. <https://doi.org/10.1016/j.matpr.2021.03.459>.
66. Gonçalves A, Cabrita R, Matos J, Rodrigues I, Vieira T, Borges JP, Soares PIP. Dual-stimuli-responsive poly(Vinyl Alcohol) nanofibers for localized cancer treatment: magnetic hyperthermia and drug release studies. *J Drug Deliv Sci Technol*. 2024;94: 105492. <https://doi.org/10.1016/j.jddst.2024.105492>.
67. Kumar S, Cherwoo L, Puri N, Sharma A, Thombare N, Bhonekar AP. Shellac: A Natural Lipid Polymer for Food Safety and Quality Monitoring. In *Nanotechnology Applications for Food Safety and Quality Monitoring*; Elsevier; 2023. p. 135–54.
68. Ji Y, Yang X, Ji Z, Zhu L, Ma N, Chen D, Jia X, Tang J, Cao Y. DFT-calculated IR spectrum amide I, II, and III band contributions of *N*-methylacetamide fine components. *ACS Omega*. 2020;5:8572–8. <https://doi.org/10.1021/acsomega.9b04421>.
69. Kandi R, Pandey PM, Majood M, Mohanty S. Fabrication and characterization of customized tubular scaffolds for tracheal tissue engineering by using solvent based 3D printing on predefined template. *Rapid Prototyp J*. 2021;27:421–8. <https://doi.org/10.1108/RPJ-08-2020-0186>.
70. Burugapalli K, Wijesuriya S, Wang N, Song W. Biomimetic electrospun coatings increase the in vivo sensitivity of implantable glucose biosensors. *J Biomed Mater Res A*. 2018;106:1072–81. <https://doi.org/10.1002/jbm.a.36308>.
71. Rynkowska E, Fatyeyeva K, Marais S, Kujawa J, Kujawski W. Chemically and thermally crosslinked PVA-based membranes: effect on swelling and transport behavior. *Polymers*. 2019;11(11):1799. <https://doi.org/10.3390/polym11111799>.
72. Campiglio CE, Contessi Negrini N, Farè S, Draghi L. Cross-linking strategies for electrospun gelatin scaffolds. *Materials*. 2019;12:2476. <https://doi.org/10.3390/ma12152476>.
73. Narayanan G, Shen J, Boy R, Gupta B, Tonelli A. Aliphatic polyester nanofibers functionalized with cyclodextrins and cyclodextrin-guest inclusion complexes. *Polymers (Basel)*. 2018;10:428. <https://doi.org/10.3390/polym10040428>.
74. Al-Azzam N, Alazzam A. Micropatterning of cells via adjusting surface wettability using plasma treatment and graphene oxide deposition. *PLoS ONE*. 2022;17: e0269914. <https://doi.org/10.1371/journal.pone.0269914>.
75. Sung H-J, Meredith C, Johnson C, Galis ZS. The effect of scaffold degradation rate on three-dimensional cell growth and angiogenesis. *Biomaterials*. 2004;25:5735–42. <https://doi.org/10.1016/j.biomaterials.2004.01.066>.
76. Kruse CR, Singh M, Targosinski S, Sinha I, Sørensen JA, Eriksson E, Nuutila K. The effect of PH on cell viability, cell migration, cell proliferation, wound closure, and wound reepithelialization. In vitro and in vivo study. *Wound Repair Regen*. 2017;25:260–9. <https://doi.org/10.1111/wrr.12526>.
77. Reddy MSB, Ponnamma D, Choudhary R, Sadasivuni KK. A comparative review of natural and synthetic biopolymer composite scaffolds. *Polymers (Basel)*. 2021;13:1105. <https://doi.org/10.3390/polym13071105>.
78. Breuls RGM, Jiya TU, Smit TH. Scaffold stiffness influences cell behavior: opportunities for skeletal tissue engineering. *Open Orthop J*. 2008;2:103–9. <https://doi.org/10.2174/1874325000802010103>.
79. Olsen CJ, Moreira J, Lukanidin EM, Ambartsumian NS. Human mammary fibroblasts stimulate invasion of breast cancer cells in a three-dimensional culture and increase stroma development in mouse xenografts. *BMC Cancer*. 2010;10:444. <https://doi.org/10.1186/1471-2407-10-444>.
80. Venegas-Cervera GA, Oliva AI, Avila-Ortega A, Cervantes-Uc JM, Carrillo-Cocom LM, Juarez-Moreno JA. Biocompatibility studies of polyurethane electrospun membranes based on arginine as chain extender. *J Mater Sci Mater Med*. 2021;32:104. <https://doi.org/10.1007/s10856-021-06581-z>.
81. Wu J, Hong Y. Enhancing cell infiltration of electrospun fibrous scaffolds in tissue regeneration. *Bioact Mater*. 2016;1:56–64. <https://doi.org/10.1016/j.bioactmat.2016.07.001>.
82. Huang-Lee LLH, Cheung DT, Nimni ME. Biochemical changes and cytotoxicity associated with the degradation of polymeric glutaraldehyde derived crosslinks. *J Biomed Mater Res*. 1990;24:1185–201. <https://doi.org/10.1002/jbm.820240905>.

**Publisher's Note** Springer Nature remains neutral with regard to jurisdictional claims in published maps and institutional affiliations.